A novel polydopamine-loaded copper sulfide (CuS@PDA) for activating H_2O_2 to eliminate tetracycline via $^1O_2$ dominated oxidation pathway

Zhou Shi[a], Chenxi He[a], Hao Huang[a], Xile Huang[a], Tong Hu[a], Yijia He[a], Dazhi Yang[a], Simeng Xia[a,*], Haojie Zhang[a,b,*], Lin Deng[a,*]

a. Hunan Engineering Research Center of Water Security Technology and Application, College of Civil Engineering, Hunan University, Changsha 410082, China

b. Helmholtz Centre for Environmental Research-UFZ, Department of Technical Biogeochemistry, Leipzig 04318, Germany

*Corresponding authors.

E-mail addresses: symeon@hnu.edu.cn (S. Xia); haojie.zhang@ufz.de (H. Zhang); lindeng@hnu.edu.cn (L. Deng)

Abstract

The frequently detected antibiotics in aquatic environments can induce antibiotic-resistance genes, thereby posing significant risks to both ecosystems and human health. Thus, it is imperative to remove antibiotics from water environments. We constructed a novel polydopamine-loaded copper sulfide (CuS@PDA) through a simple hydrothermal method to activate H_2O_2 to degrade tetracycline (TC). Compared to CuS/H_2O_2, the CuS@PDA/H_2O_2 system not only achieved efficient TC removal with kinetic rate constant of 0.20 min^{-1}, but also showed much lower Cu^{2+} ions leaching (3.81 mg/L from CuS *vs.* 0.21 mg/L from CuS@PDA). Besides, CuS@PDA exhibited remarkable recyclability with 93% removal in the fifth consecutive cycle. Mechanisms analysis revealed that Cu and S contributed to the H_2O_2 activation and S promoted the conversion of Cu(II) to Cu(I), beneficial for the production of reactive oxygen species. $^1O_2$ was found to play the dominant role in the degradation of TC on the basis of quenching tests and electron paramagnetic resonance (EPR) analysis. PDA in CuS@PDA composites facilitated easier complexation with H_2O_2 and conferred stronger oxidation capability. Lastly, the TC degradation pathway by CuS@PDA/H_2O_2 was proposed, and the ecotoxicity of its degradation intermediates was estimated. In conclusion, this work presents an approach for synthesizing high efficient and recyclable CuS-based catalysts that activate H_2O_2 to efficiently degrade organic pollutants through a nonradical pathway predominantly mediated by $^1O_2$.

Keywords: CuS; Polydopamine; H_2O_2 activation; Tetracycline degradation; $^1O_2$ dominated

1. Introduction

The presence of pharmaceutical and personal care products in aquatic environment leads to severe ecological risks such as endocrine disruption and bioaccumulation [1]. Tetracyclines (TC), extensively used in aquaculture and veterinary medicine [2], has been frequently detected in surface water, groundwater, and municipal wastewater due to its hydrophilicity, weak volatility, and high adsorptive capacity [3]. This poses serious threat to human health, induces bacteria resistance, and endangers the ecological environment [4]. Conventional water and wastewater treatment methods such as flocculation, precipitation, adsorption, and activated sludge process fail to efficiently remove TC from aqueous solutions [5]. Thus, it's urgent to find effective and environmental-friendly strategies to deal with the intractable problems of antibiotic pollution.

In recent years, advanced oxidation processes (AOPs) that can generate reactive oxygen species (ROS, such as •OH, $SO_4^{-\bullet}$, etc.) have been considered as one of the most promising techniques to eliminate refractory organic pollutants [6]. The high oxidation ability of ROS can decompose the targeted pollutants into small molecules with low-toxicity, and even mineralize them into CO_2 and H_2O [7]. The Fenton/Fenton-like processes, based on H_2O_2 activation, has garnered increasing attention due to their advantages of simplicity in operation, high effectiveness, mild reaction conditions, and environmental friendliness [8]. The commonly employed activation approaches encompass photocatalysis [9,10], electrocatalysis [11], transition metals (i.e. Fe [12], Co [13], Cu [14], Mn [15], etc), carbon [16] and bimetallic metals catalysts activation [17].

Due to the significantly higher reaction rate constant of Cu(I) with H_2O_2 (10^4 M^{-1} S^{-1}) compared to Fe(II) (76 M^{-1} S^{-1}), various solid catalysts containing copper have

been employed as alternatives to iron-based catalysts [18], including zero valent copper [19], copper oxides [20], and copper-based composites [21]. Copper sulfide (CuS) has drawn considerable attention due to the weaker bonding energy between Cu and S compared to Cu and O, which can effectively improve the catalytic reaction rate [22]. Additionally, sulfur species (S^{2-}, S_n^{2-}) present in CuS can facilitate the reduction of high-valence Cu to low-valence Cu, thereby significantly enhancing the catalytic activity as well [23]. However, the Cu^{2+} ions leakage from CuS during the catalytic reaction in pollutants removal greatly inhibits its practical application.

Dopamine (DA) is a molecule containing amine and catechol functional groups [24], which can undergo self-polymerization reaction in a simple environment to produce polydopamine (PDA) [25]. PDA possesses abundant functional groups such as carboxyl groups, amino groups, and π-π bond. These functional groups make it an excellent in-situ reduction reagent for metal nanoparticles [26], as well as an anchorage point for metal-based materials to construct various secondary reaction platforms. Moreover, these groups can establish strong interactions including hydrogen bonding, electrostatic interactions, and π-π interactions to enhance the adsorption properties of carriers for catalysts and pollutants [27]. Besides, the π-π stacked PDA coating exhibits favorable electrochemical property that significantly accelerate the electron transfer rate [24,25]. Utilizing PDA as a modification carrier enables uniform distribution of metal particles, increased surface area, and generation of nanostructured catalysts with enhanced stability and catalytic efficiency [28].

Considering all the above-mentioned points, we speculated that the introduction of PDA onto CuS to synthesize CuS@PDA composite could prevent the copper ions leaching, making it a high-effective, structure stable and recyclable H_2O_2 activator. Nevertheless, to the best of our knowledge, the application of CuS@PDA in H_2O_2

activation for refractory organic pollutants degradation has rarely been reported. Herein, spherical CuS@PDA composites were synthesized via a hydrothermal method. The morphology, crystal structure, and chemical composition of CuS@PDA were systematically characterized. The catalytic activity of CuS@PDA in activating H_2O_2 for TC degradation was investigated with respect to several key parameters, including initial pH, H_2O_2 concentration, CuS@PDA dosage, and co-existing inorganic anions. Besides, electron paramagnetic resonance (EPR) analysis and quenching experiments were performed to elucidate the production and contribution ratios of ROS to the degradation. The mechanisms underlying TC degradation by CuS@PDA/H_2O_2 were proposed, and the degradation intermediates and pathways were identified as well.

2. Experimental methods

2.1. Chemicals

Tetracycline (TC), Sulfadiazine (SDZ), carbamazepine (CBZ), Tris (hydroxymethyl) aminomethane Hydrochloride (Tris-HCl), tert-butanol (TBA), L-histidine (l-his), NaF, furfuryl alcohol (FFA) were provided by Macklin Biochemical Technology Co. Ltd. (Shanghai, China). Sulfamethoxazole (SMX), coumarin (CM), hydrogen peroxide (H_2O_2, 30%), ethyl alcohol (EtOH), methanol (MeOH), 1.4-benzo-quinone (BQ), 5,5-Dimethyl-1-pyrroline N-oxide (DMPO), 2,2,6,6-tetra-methyl-4-piperidone (TEMP) were obtained from Sigma-Aldrich Chemical Co. Ltd. (China). Dopamine hydrochloride (DA) and $CuCl_2$•$2H_2O$ were supplied by Aladdin Biological Technology Co. Ltd. (Shanghai, China). Thiourea (CH_4N_2S), Potassiumperiodate (KIO_4), NaOH, HCl, NaCl, $NaNO_3$, Na_2SO_4, $NaHCO_3$, NaH_2PO_4 were purchased from Sinopharm Chemical Reagent Co. Ltd. (Shanghai, China). All chemicals were of at least analytical grade and used without further purification. Ultrapure water (18.2 MΩ · cm) used throughout the study was prepared using a Millipore system (Bedford, USA).

2.2. Catalysts synthesis and characterization

The CuS@PDA composite was synthesized via a facile hydrothermal method, as illustrated in Figure 1a. Initially, a precise amount of Tris-HCl (10 mM) weighing 145 mg was dissolved in 80 mL of ultrapure water to prepare solution A. Subsequently, solution B was prepared by dissolving 204 mg of $CuCl_2 \cdot 2H_2O$ accurately weighed in 40 mL of ultrapure water. Then, under magnetic stirring and pH adjustment to 8.5, solution A was supplemented with 232 mg of DA while simultaneously introducing CH_4N_2S weighing 91 mg into solution B with continuous stirring. After a reaction time of 30 min, solution B was poured into solution A and the resulting mixture was stirred for an additional duration of 24 h until it attained a grayish white coloration. The reaction mixture was transferred to an autoclave and maintained at a temperature of 120℃ for a period of 12 h. Upon cooling to room temperature, the solids were collected by filtration and thoroughly rinsed multiple times with deionized water. Finally, the solids were vacuum dried at 60℃ for 12 h to obtain CuS@PDA composites. PDA and CuS were prepared following the identical procedure as CuS@PDA but without adding $CuCl_2 \cdot 2H_2O$ and DA, respectively.

The analytical and characterization methods are described in Text S1.

2.3. Degradation tests of TC

The degradation experiments were conducted in a series of 100 mL glass beakers. Typically, 5 mg of catalyst was mixed with 50 mL of a 40 μM TC solution and dispersed ultrasonically for 1 min. Subsequently, 5 mM H_2O_2 was added to initiate the degradation process. At predetermined time intervals, 0.5 mL of the solution was withdrawn, followed by filtration through a 0.22 μm membrane filter and immediate quenching with methanol (0.2 mL). The residual TC concentration in the solution was analyzed using high-performance liquid chromatography (HPLC). The initial pH of the

TC solution was adjusted using HCl or NaOH if necessary. To ensure experimental accuracy, all experiments were performed in triplicate and the results were reported as mean values with standard deviations.

3. Results and discussion

3.1. Characterization

The microstructure and surface morphology of CuS, PDA, and CuS@PDA were characterized using SEM and TEM images. As shown in Figure 1b and e, CuS exhibits a tubular flower-like morphology composed of nanosheets. On the other hand, PDA possesses a uniform nanospherical structure with a smooth surface, having an average diameter of approximately 200-500 nm (Figure 1c and f). In contrast, CuS@PDA maintains its spherical structure but displays a rougher morphology with smaller particle size and more pronounced agglomeration (Figure 1d). The TEM image in Figure 1g clearly reveals that the prepared CuS@PDA consists of randomly assembled nanorods. Additionally, the HRTEM image of CuS@PDA in Figure 2h exhibits uniformly distributed lattice fringes measuring at 0.305, 0.190, and 0.281 nm, corresponding to the (102), (110), and (103) crystal faces of the CuS nanocrystals respectively [29,30]. EDS elemental mapping also confirms that both Cu and S are evenly distributed throughout the material as shown in Figure 1i.

XRD patterns were utilized to analyze the crystalline structure of CuS, PDA, and CuS@PDA as depicted in Figure 2a. The characteristic peaks of CuS@PDA observed at 2θ of 27.7°, 29.3°, 31.8°, 32.9°, 48.0°, 52.7°, and 59.3° can be indexed to the (101), (102), (103), (006), (110), (108) and (116) planes of CuS (JCPDS 20−0534), respectively. This indicates a well-defined crystalline structure of CuS grown on the PDA matrix [31,32]. The intensity of overlapped peaks for both (103) and (006) is much weaker than that for (110), which suggests preferential growth along the direction (110)

and polysulfide formation in CuS [33]. Compared to the pure CuS, the intensity of some diffraction peaks in CuS@PDA is slightly reduced, and this can be related to the surface modification by PDA on specific crystalline surfaces of CuS [34]. The Brunauer-Emmett-Teller (BET) and specific surface areas (S_{BET}) of CuS@PDA were examined by N_2 adsorption/desorption isotherms. As shown in Figure 2b, CuS@PDA displays a typical IV-type isotherm accompanied by a H3 hysteresis loop, indicating the presence of mesoporous structure. The S_{BET} of CuS@PDA was calculated to be 55.67 m^2/g, with a total pore volume of 0.21 cm^3/g and average pore diameter of ~15 nm (Figure 2c). The surface functional groups of CuS, PDA, and CuS@PDA were analyzed by FTIR. As depicted in Figure 2d, the pure PDA exhibits several characteristic absorption peaks at 1290, 1512, 1618, and 3100-3600 cm^{-1}, corresponding to the C−O stretching vibration, N−H shear vibration, N−H bending vibration [35], and O−H stretching vibration of surface hydroxyl groups, respectively [36]. In the FTIR spectrum of CuS, the absorption peak at 612 cm^{-1} can be assigned to the Cu−S stretching vibration [37], and the peak centered at 1109 cm^{-1} is related to the S−O stretching vibration [38]. Obviously, the as-synthesized CuS@PDA possesses the characteristic peaks of both CuS and PDA. Due to the encapsulation of PDA, the Cu−S bond weakens, and the S−O bond disappears. The results indicate that CuS@PDA was successfully prepared. These results demonstrate the successful synthesis of CuS@PDA.

3.2. Catalytic activity tests

The catalytic activity of CuS@PDA in activating H_2O_2 for TC degradation is demonstrated in Figure 3. As shown in Figure 3a, the individual utilization of H_2O_2 or PDA exhibited negligible TC removal within a 30 min timeframe, indicating that the direct oxidation failed to achieve satisfactory TC removal and the adsorption capacity of PDA was insignificant. The removal efficiency achieved by CuS reached 37.2%, and

193 it increased to 58.4% when using CuS@PDA as the adsorbent. As expected,
194 simultaneous addition of H_2O_2 (5 mM) and CuS@PDA (0.1 g/L) resulted in accelerated
195 TC removal. As shown in Figure 3b, the pseudo-first-order kinetic rate constant (k)
196 obtained by CuS@PDA/H_2O_2 was determined to be 0.20 min^{-1}, higher than that
197 obtained by CuS/H_2O_2 (0.12 min^{-1}). Further, the presence of 0.1 g/L PDA in CuS/H_2O_2
198 system improved the k value from 0.12 to 0.15 min^{-1}, indicating its promotion effect to
199 degrade TC. Overall, the as-synthesized CuS@PDA exhibited the highest catalytic
200 activity while effectively mitigating Cu ions leaching compared to other catalysts tested
201 as illustrated in Figure 3c. It's worth noting that the leaching concentrations of Cu^{2+}
202 ions in the CuS@PDA/H_2O_2 system was only 0.2 mg/L, significantly lower than the
203 integrated tap-water standard of U.S. Environmental Protection Agency (1.3 mg/L).
204 While the leaching concentration of Cu^{2+} ions in the CuS/H_2O_2 system was 3.81 mg/L.
205 Obviously, the incorporation of PDA effectively alleviated the release of Cu^{2+} from CuS,
206 which is advantageous for practical application. Table S2 compares the kinetic rate
207 constants of TC degradation by different catalysts in H_2O_2-based AOPs. As observed,
208 CuS@PDA demonstrates a much higher k value compared to the reported catalysts.
209 The recyclability of solid catalysts are crucial characteristics for their practical
210 application. In this study, five consecutive cycling tests were conducted to compare the
211 recyclability of CuS@PDA and CuS. After each cycle, the solid catalyst was collected,
212 washed with ethanol and ultrapure water, vacuum dried, and subsequently reused. As
213 shown in Figure 3d, the degradation of TC reduced to 73% in the fifth run when using
214 CuS as the catalyst due to the reduced active sites caused by copper ions leakage from
215 CuS. In contrast, CuS@PDA consistently maintained a removal efficiency 93% after
216 five repeated cycles.
217 These findings demonstrated that CuS@PDA exhibited high efficiency,

exceptional recyclability and structural stability, thereby potentially reducing environmental organic pollutants.

3.3. Influencing factors on TC degradation

The influences of operational parameters (i.e., CuS@PDA dosage, H_2O_2 concentration, initial pH, and coexisting anions) on TC removal by the CuS@PDA activated H_2O_2 system are discussed in the following section. Figure 4a illustrates the impact of catalyst dosage (0, 5, 8, 10, and 13 mg). It is evident that different catalyst dosages have varying effects on the removal efficiency of TC. In the absence of CuS@PDA in the solution, the removal was minimal, indicating that the self-decomposition of H_2O_2 was ineffective. Conversely, when 5 mg of CuS@PDA presented, 94.46% of TC was removed in 30 min. This was related to the surface active sites on the catalyst that could rapidly activate H_2O_2 to produce high-effective active substances to degrade TC [39]. Yet, further increase in catalyst dosage from 10 to 13 mg led to a declined degradation rate, which was related to the self-quenching effect caused by excess radicals and diffusion limitation caused by excess catalyst [40]. Considering the removal efficiency and cost control, the optimum dosage of 5 mg CuS@PDA was selected in the subsequent tests. The H_2O_2 concentration also played a pivotal role in the degradation of TC by CuS@PDA/H_2O_2. As shown in Figure 4b, the removal efficiency was limited to approximately 58.4% in the absence of H_2O_2. However, with the addition of 1 mM H_2O_2, the degradation rapidly improved to 86.5%. Furthermore, a gradual enhancement in degradation was observed as the H_2O_2 concentration increased from 1 to 10 mM. Ultimately, an optimum H_2O_2 concentration of 5 mM was selected.

The initial solution pH also impacts the performance heterogeneous catalysis in the degradation of organic pollutants. As shown in Figure 4c, an extremely acidic

condition (pH=3) was found to be unfavorable for TC degradation. Nevertheless, a high removal efficiency above 90% was maintained across a wide pH range of 5−11, indicating that CuS@PDA can be practically utilized without requiring pH adjustment. At low pH, H^+ can serve as a scavenger for •OH via equation of $H^+ + •OH + e^+ \rightarrow H_2O$ [41]. Additionally, literature reports suggest that the increasing electron density in the TC^- and TC^{2-} ring systems with rising pH promotes direct decomposition of TC molecules through the direct attack of H_2O_2 and free radicals [42]. To gain a deeper understanding of the influence of initial pH on TC removal, the zeta potential of CuS@PDA at various pH levels was recorded as depicted in Figure S1. The surface charge of CuS@PDA was negative within the tested pH range, which was primarily induced by imine, quinone, and catechol groups on PDA [43]. Besides, the deprotonation/protonation and reversible dissociation of catechol groups and amines also contributed to the negative charge on CuS@PDA as reported previously [44]. These findings suggest that the electrostatic force might played a minor role in the degradation of TC.

Considering the presence of various inorganic anions (Cl^-, NO_3^-, SO_4^{2-}, $H_2PO_4^-$, and HCO_3^-) in natural water, their impact on TC degradation was investigated as shown in Figure 4d. The degradation was inhibited by 9% when 20 mM Cl^- was present due to the generation of less reactive $ClOH^{•-}$ ($•OH + Cl^- \rightarrow ClOH^{•-}$) [45]. The inhibiting effect of 20 mM NO_3^- could be attributed to the competition between NO_3^- and TC for adsorption sites on CuS@PDA. SO_4^{2-} can be adsorbed on the catalyst surface and compete with TC molecules for active site, thereby hindering TC degradation [39,46]. $H_2PO_4^-$ exhibits a quenching effect on •OH through the formation of low-active $H_2PO_4^{•-}$, consequently impeding the degradation. Although HCO_3^- is considered as a scavenger of •OH ($k = 8.5 \times 10^6\ M^{-1}s^{-1}$) [39,47], it actually promoted the degradation

in this study due to the production of •OH and $^1O_2$ from HCO_3^- [48]. Nevertheless, even in the presence of excessive inorganic anions the CuS@PDA/H_2O_2 system still achieved ~80% TC removal, suggesting its robustness and suitability for actual application.

3.5. Mechanisms understanding of TC degradation by CuS@PDA/H_2O_2

3.5.1. Identification of possible reactive species

Quenching tests and electron paramagnetic resonance (EPR) were applied to uncover the reactive oxygen species (ROS) responsible for TC degradation in the CuS@PDA/H_2O_2 system. Tert-butanol (TBA) is an effective scavenger of •OH with quenching rate of $(3.8–7.6)\times10^7$ M^{-1} s^{-1}, while *p*-benzoquinone (BQ) and L-histidine (L-his) can act as quenchers of $O_2^{\bullet-}$ [$(0.9–1.9)\times10^7$ M^{-1} s^{-1}] and $^1O_2$ (3.2×10^7 M^{-1} s^{-1}), respectively [49,50]. NaF is a typical quenching agent for surface bound free radicals on the catalyst surface in heterogeneous catalysis [49]. As shown in Figure 5a, in contrast to the control group without scavengers addition, the presence of 200 mM TBA inhibited a slightly inhibitory effect on the degradation. Even with an increased TBA concentration of 1 M, TC removal only dropped to 77.4%, indicating that •OH played a minor role in TC oxidation. Furthermore, instead of inhibition, the inclusion of 20 mM BQ demonstrated a promotional effect, suggesting that $O_2^{\bullet-}$ might not serve as the primary active species for the degradation either. As illustrated in Figure 5b, the introduction of 10 mM NaF had no impact on the degradation, implying that surface-bound free radicals had negligible influence on the degradation of TC [51]. In comparison, the addition of 100 mM L-his suppressed the degradation to 60%. Yet, the inhibitory effect of L-his does not provide direct evidence for the involvement of $^1O_2$ as the main reactive species since L-his can readily form a complex with Cu(II), thereby obstructing ROS formation [52]. A pronounced quenching effect was also observed for

furfuryl alcohol (FFA). This tentatively indicated that the degradation of TC did not rely on free radials, with $^1O_2$ being the major contributor.

To ascertain the production of Cu(III) in the CuS@PDA/H_2O_2 system, periodate was used as a chemical probe for Cu(III) [40,53]. Surprisingly, the presence of 1 mM periodate sharply expedited the degradation (Figure 5b). This observation suggested that periodate did not complex with Cu(III), but rather functioned as an oxidizing agent to facilitate the degradation. The formation of Cu(III) was excluded.

To further validate the quenching tests results, EPR analysis using DMPO and TEMP as spin trapping agents were further conducted to identify the formed ROS in the CuS@PDA/H_2O_2 system. As depicted in Figure 5c, d, and e, no signal was found in the absence of H_2O_2, demonstrating that CuS@PDA itself can not produce ROS. In contrast, characteristic peaks of DMPO-•OH (1:2:2:1), DMPO-$O_2^{\bullet-}$ (1:2:2:1), and TEMP-$^1O_2$ (1:1:1) appeared with the coexistence of CuS@PDA and H_2O_2, further validating the generation of •OH, $O_2^{\bullet-}$, and $^1O_2$. As the reaction time prolonged, the peak intensity enhanced gradually, verifying the continuously production of ROS by CuS@PDA/H_2O_2. Thus, the above results conclusively indicated that $^1O_2$ plays a major role in the degradation.

Further investigations into the generation of $^1O_2$ in the CuS@PDA/H_2O_2 system was performed to understand the underlying processes as dissolved oxygen [54], light irradiation [55] and $O_2^{\bullet-}$ reorganization [40] have been reported to be responsible for $^1O_2$ production. As shown in Figure S2, the degradation was barely influenced under continuous N_2 pumping and dark conditions, which ruled out dissolved oxygen as a precursor of $^1O_2$. Combining with the result in Figure 5a that $O_2^{\bullet-}$ did not contribute to the degradation, it was concluded that $^1O_2$ mainly originated from H_2O_2 and rather than the recombination of $O_2^{\bullet-}$.

318 3.5.2. The role of PDA

319 To examine the role of PDA on the enhanced catalytic activity of CuS@PDA, the
320 electrochemical responses of PDA, CuS, and CuS@PDA towards H_2O_2 and TC were
321 recorded by determining the open-circuit potential (OCP), as shown in Figure 5f. The
322 OCP values exhibited by PDA, CuS, and CuS@PDA were found to be 0.088, 0.26, and
323 0.24 V, respectively. The enhanced content of pyridinc and pyrrolic N in CuS@PDA
324 resulting from the introduction of PDA facilitated easier complexation with H_2O_2 and
325 conferred stronger oxidation capability [56]. Thus, upon addition of H_2O_2, the OCP of
326 CuS@PDA abruptly improved from 0.24 to 0.43 V owing to the elevated potential
327 associated with formed H_2O_2 complexes. While, regarding to CuS, it only increased by
328 0.1 V (from 0.26 to 0.36 V). Subsequently, the OCP value gradually decreased by 0.016
329 V following TC injection due to the decomposition of surface complexes. The
330 CuS@PDA displayed a more pronounced decline in OCP, indicating that active
331 complexes formed on its surface possessed superior oxidation ability towards TC
332 compared to those formed on CuS.

333 Furthermore, the FTIR spectrum of the fresh and used CuS@PDA was recorded
334 to determine the change in surface functional groups. As shown in Figure 6a, after the
335 catalytic reaction, the absorption peak corresponding to N−H bending vibration shifted
336 from 1618 to 1579 cm^{-1}, and the peak belonging to N−H scissoring vibration at 1439
337 cm^{-1} enhanced significantly, suggesting the participation of N−H in the catalytic
338 degradation of TC in the studied CuS@PDA/H_2O_2 system. The peak related to Cu−S
339 bond also shifted from 612 to 608 cm^{-1}, which evidenced the involvement Cu−S.

340 3.5.3. Mechanism investigation of TC degradation by CuS@PDA/H_2O_2

341 To further elucidate the mechanisms underlying TC degradation by
342 CuS@PDA/H_2O_2, XPS analysis was conducted to determine the chemical composition

and valence states of both fresh and used CuS@PDA. Figure 6b presents the full-scale XPS spectra, which clearly indicates the presence of Cu, O, N, C, and S elements in the as-synthesized CuS@PDA. The high-resolution N 1s spectrum (Figure 6c) was deconvoluted into three distinct peaks corresponding to imino groups, substituted amines, and amine groups at binding energies of 398.8, 399.8, and 400.7 eV, respectively [31]. These peaks primarily originate from the indole or indoline structure in PDA [57]. XPS analysis of Cu displays two main peaks at binding energies of 932.6 eV and 952.6 eV (Figure 6d), belonging to Cu $2p_{3/2}$ and Cu $2p_{1/2}$ spin orbitals, respectively [58]. The Cu $2p_{3/2}$ spectrum is further resolved into two individual peaks, with Cu(I) appearing at 932.2 eV and Cu(II) at 933.2 eV. As seen, the Cu 2p XPS spectrum of CuS@PDA exhibits remarkable similarity to that of CuS, indicating the relatively stability of copper element in CuS during the complexation process with DA. Regarding the high-resolution S 2p spectrum (Figure 6e), the peaks observed at 161.5 eV and 163.4 eV can be assigned to sulfide ions (S^{2-}) and polysulfide (S_n^{2-}), respectively [39,59]. The peaks centered at 164.4 eV and 168.6 eV correspond to elemental sulfur (S^0) and sulfate ions, respectively [39,59,60]. In contrast with CuS, the absence of S^0 peak and presence of sulfate ions peak in CuS@PDA may be attributed to the oxidation of CuS during the self-polymerization process of DA [60].

Obviously, after activating H_2O_2 for TC degradation, the relative proportion of Cu(II) in CuS@PDA reduced from 50.37% to 37.41%, accompanied by an increase in the proportion of Cu(I) from 49.63% to 62.59%. This shift indicated a transition in oxidation state from Cu(II) to Cu(I), providing evidence for the involvement of Cu(II) in the catalytic process. On the other hand, there was a significant decline in the relative proportion of S^{2-} from 84.46% to 19.82%, while varying degrees of increases were observed in the S_n^{2-}, S^0, and sulfate content, suggesting the participation of S^{2-} in the

catalytic process. The XPS analysis revealed the involvement of both Cu and S, with S exhibiting an accelerating effect on the conversion of Cu(II) to Cu(I) [61].

Based on the preceding discussion, a possible mechanism of TC degradation by the CuS@PDA activated H_2O_2 system was proposed as schematically in Figure 7. As H_2O_2 molecule reached the surface of CuS@PDA, the exposed Cu active site on which underwent redox cycle with H_2O_2 according to Eqs.1 and 2 [62,63]. However, the slow reaction rate between Cu(II) and H_2O_2 greatly affected the regeneration of Cu(I) [64]. Fortunately, the presence of sulfur in CuS@PDA expedited the conversion of Cu(II) to Cu(I) according to Eq. 3, thereby accelerating the production of •OH (Eq. 2) [62]. $^1O_2$ was considered as the predominant ROS contributing to the degradation of TC. The generation of $^1O_2$ from H_2O_2 can occur via either a one-step two-electron or a two-step one-electron transfer pathway [65]. Based on quenching tests and the Haber-Weiss cycle theory, two-step one-electron transfer was supposed to be a reliable pathway for $^1O_2$ production [66]. The first one-electron pathway yielded HOO•/$O_2^{\bullet-}$ via Eq. 4, where an electron was transferred from H_2O_2 to Cu(II) (Eq. 1). Subsequently, $O_2^{\bullet-}$ was produced from HOO• through Eq. 5 [66]. The second one-electron pathway entailed $^1O_2$ generation from HOO•/$O_2^{\bullet-}$ and encompassed three possible routes: rapid oxidation of spin-state Cu(II) by the generated HOO•/$O_2^{\bullet-}$ (Eq. 6), reactive species reactions involving recombination of HOO• and reactions between HOO•, $O_2^{\bullet-}$, and •OH according to Eqs. 7-10 [65,67], and reactions between H_2O_2 with HOO•/$O_2^{\bullet-}$ (Eqs. 11 and 12) [68].

$$Cu(II) + H_2O_2 \rightarrow Cu(I) + H^+ + HOO\bullet \quad (1)$$

$$Cu(I) + H_2O_2 \rightarrow Cu(II) + OH^- + \bullet OH \quad (2)$$

$$Cu(II) + S^{2-} + 4H_2O \rightarrow Cu(I) + SO_4^{2-} + 8H^+ \quad (3)$$

$$Cu(II) + H_2O_2 \rightarrow Cu(I) + HOO\bullet/O_2^{\bullet-} + H^+ \quad (4)$$

$$HOO\bullet \rightarrow O_2^{\bullet-} + H^+ \quad (5)$$

$$Cu(II) + HOO\bullet/O_2^{\bullet-} \rightarrow Cu(I) + {}^1O_2 + H^+ \quad (6)$$

$$HOO\bullet + HOO\bullet \rightarrow {}^1O_2 + H_2O_2 \quad (7)$$

$$HOO\bullet + \bullet OH \rightarrow {}^1O_2 + H_2O \quad (8)$$

$$O_2^{\bullet-} + \bullet OH \rightarrow {}^1O_2 + OH^- \quad (9)$$

$$O_2^{\bullet-} + HOO\bullet \rightarrow HO_2^- + {}^1O_2 \quad (10)$$

$$HOO\bullet + H_2O_2 \rightarrow H_2O + \bullet OH + {}^1O_2 \quad (11)$$

$$O_2^{\bullet-} + H_2O_2 \rightarrow OH^- + \bullet OH + {}^1O_2 \quad (12)$$

3.6. Degradation pathways and toxicity analysis of intermediates

A total of eighteen intermediates of TC degradation by CuS@PDA/H_2O_2 were identified as shown in Figure S3 and Table S3. Three potential degradation pathways including terminal oxidation, dealkylation, deamination and ring-opening reactions were proposed in Figure 8 [69]. In pathway 1, TC underwent terminal oxidation to generate the intermediate P7 (m/z=475), which was subsequently degraded into p9 (m/z=360) through dealkylation and disruption of the benzene ring [70]. The ring cleavage under $^1O_2$ attack led to the formation of P10, P11, and P12 [71]. In pathway 2, nucleophilic reactions occurred to produce P1 (m/z=461) and P2 (m/z=477), followed by dehydrogenation under $O_2^{\bullet-}$ attack to form a downstream intermediate P3 (m/z=459) [72]. In pathway 3, TC was attacked by ROS to produce P4 (m/z=417) via an N-demethylation process [73], which further underwent amide group destruction, demethylation, and dehydroxylation to produce P5 (m/z=339) and P6 (m/z=325). Thereafter, a ring-opening reaction occurred yielding P7 (m/z=171) [74]. Additionally, several small molecules including P13 (m/z=262), P14 (m/z=223) [72], P15 (m/z=132) [74], P16 (m/z=118) [75], P17 (m/z=90) and P18 (m/z=60) [73] were detected as well. All intermediates could be further decomposed into low molecular compounds such as

H_2O, CO_2, and NO_3^- via subsequent reactions with $^1O_2$, •OH and $O_2^{\bullet-}$ [69,76,77].

The developmental toxicity and mutagenic toxicity of TC and main degradation intermediates were predicted and assessed through Toxicity Estimation Software (T.E.S.T.) based on quantitative structure-activity relationship (QSAQ) as shown in Figure S4. TC has significant developmental toxicity (0.86) and positive mutagenic toxicity (0.6). Compared to the parent TC, the toxicity of most intermediates declined. As shown in Figure S4a, apart from P4 and P6, the developmental toxicity of other intermediates was reduced. Similarly, most intermediates exhibited a reduction in mutagenicity (Figure S4b). Thus, it could be deduced that the CuS@PDA/H_2O_2 system not only efficiently eliminated TC, but also mitigated the toxicity of degradation intermediates during the degradation. This was of great significance for the safety of water environment.

4. Conclusions

In this study, CuS@PDA composite was synthesized via a simple hydrothermal method using DA and CuS, aiming for activating H_2O_2 to remove TC from aqueous solutions. The degradation tests results showed that a removal efficiency of 94.9% was achieved within 30 min in the presence of 0.1 g/L CuS@PDA and 5 mM H_2O_2. The as-synthesized CuS@PDA not only exhibited excellent catalytic activity within a wide pH range from 5 to 11, bu also showed remarkable recyclability with 93% removal in the fifth consecutive cycle. Quenching experiments and EPR analysis confirmed that $^1O_2$ played a crucial role in the degradation of TC. Mechanistic analysis revealed that S in CuS@PDA facilitated the Cu(II)/Cu(I) redox cycle, with H_2O_2 serving as the main source for generating $^1O_2$. Further, the degradation pathways and intermediate toxicity of TC were also studied. In conclusion, this study presents an efficient and recyclable CuS@PDA composite to activate H_2O_2 for refractory organic pollutants removal in

443 water and wastewater treatments.

444

445 **Acknowledgments**

446 This work was financially supported by National Natural Science Foundation of China

447 (52270004).

448

Reference

[1] Current research trends on emerging contaminants pharmaceutical and personal care products (PPCPs): A comprehensive review, Sci. Total Environ. 859 (2023) 160031. https://doi.org/10.1016/j.scitotenv.2022.160031.

[2] J.J. López Peñalver, C.V. Gómez Pacheco, M. Sánchez Polo, J. Rivera Utrilla, Degradation of tetracyclines in different water matrices by advanced oxidation/reduction processes based on gamma radiation, J. Chem. Technol. Biotechnol. 88 (2013) 1096–1108. https://doi.org/10.1002/jctb.3946.

[3] R. Daghrir, P. Drogui, Tetracycline antibiotics in the environment: a review, Environ. Chem. Lett. 11 (2013) 209–227. https://doi.org/10.1007/s10311-013-0404-8.

[4] Y. Amangelsin, Y. Semenova, M. Dadar, M. Aljofan, G. Bjørklund, The Impact of Tetracycline Pollution on the Aquatic Environment and Removal Strategies, Antibiotics 12 (2023) 440. https://doi.org/10.3390/antibiotics12030440.

[5] K. Ming, F. Chen, L. Zhu, S. Xia, L. Yang, Z. Shi, L. Deng, H. Zhang, Perborate accelerated copper-immobilized carbon nanofibers activating peroxymonosulfate process for sulfadiazine degradation: Performance and mechanisms understanding, Sep. Purif. Technol. 324 (2023) 124587. https://doi.org/10.1016/j.seppur.2023.124587.

[6] Z. Cheng, L. Ling, Z. Wu, J. Fang, P. Westerhoff, C. Shang, Novel Visible Light-Driven Photocatalytic Chlorine Activation Process for Carbamazepine Degradation in Drinking Water, Environ. Sci. Technol. 54 (2020) 11584–11593. https://doi.org/10.1021/acs.est.0c03170.

[7] F. Ahmad, D. Zhu, J. Sun, Environmental fate of tetracycline antibiotics: degradation pathway mechanisms, challenges, and perspectives, Environ. Sci. Eur. 33 (2021) 64. https://doi.org/10.1186/s12302-021-00505-y.

[8] Y. Liu, Y. Zhao, J. Wang, Fenton/Fenton-like processes with in-situ production of hydrogen peroxide/hydroxyl radical for degradation of emerging contaminants: Advances and prospects, J. Hazard. Mater. 404 (2021) 124191. https://doi.org/10.1016/j.jhazmat.2020.124191.

[9] Y. Huang, M. Kong, S. Coffin, K.H. Cochran, D.C. Westerman, D. Schlenk, S.D. Richardson, L. Lei, D.D. Dionysiou, Degradation of contaminants of emerging concern by UV/H2O2 for water reuse: Kinetics, mechanisms, and cytotoxicity analysis, Water Res. 174 (2020) 115587. https://doi.org/10.1016/j.watres.2020.115587.

[10] IJERPH | Free Full-Text | Removal of Sulfamethoxazole, Sulfathiazole and Sulfamethazine in their Mixed Solution by UV/H2O2 Process, (n.d.). https://www.mdpi.com/1660-4601/16/10/1797 (accessed June 17, 2024).

[11] Y. Zhu, F. Deng, S. Qiu, F. Ma, Y. Zheng, R. Lian, Enhanced electro-Fenton degradation of sulfonamides using the N, S co-doped cathode: Mechanism for H2O2 formation and pollutants decay, J. Hazard. Mater. 403 (2021) 123950. https://doi.org/10.1016/j.jhazmat.2020.123950.

[12] Y. Qu, Z. Chen, Y. Duan, L. Liu, H2O2 assisted photocatalysis over Fe-MOF modified BiOBr for degradation of RhB, J. Chem. Technol. Biotechnol. 97 (2022) 2881–2888. https://doi.org/10.1002/jctb.7199.

[13] X. Long, Z. Yang, H. Wang, M. Chen, K. Peng, Q. Zeng, A. Xu, Selective Degradation of Orange II with the Cobalt(II)–Bicarbonate–Hydrogen Peroxide System, Ind. Eng. Chem. Res. 51 (2012) 11998–12003. https://doi.org/10.1021/ie3013924.

[14] C. Meng, Z. Wang, W. Zhang, L. Cui, B. Yang, H. Xie, Z. Zhang, Laminar membranes assembled by ultrathin cobalt-copper oxide nanosheets for nanoconfined catalytic degradation of contaminants,

Chem. Eng. J. 449 (2022) 137811. https://doi.org/10.1016/j.cej.2022.137811.
[15] L. Chen, T. Maqbool, C. Hou, W. Fu, X. Zhang, Mechanistic study of oxidative removal of bisphenol A by pristine nanocatalyst MnO/peroxymonosulfate34, Sep. Purif. Technol. 281 (2022) 119882. https://doi.org/10.1016/j.seppur.2021.119882.
[16] X. Zhang, P. Sun, K. Wei, X. Huang, X. Zhang, Enhanced H2O2 activation and sulfamethoxazole degradation by Fe-impregnated biochar, Chem. Eng. J. 385 (2020) 123921. https://doi.org/10.1016/j.cej.2019.123921.
[17] N. Li, X. He, J. Ye, H. Dai, W. Peng, Z. Cheng, B. Yan, G. Chen, S. Wang, H2O2 activation and contaminants removal in heterogeneous Fenton-like systems, J. Hazard. Mater. 458 (2023) 131926. https://doi.org/10.1016/j.jhazmat.2023.131926.
[18] J. Li, A.N. Pham, R. Dai, Z. Wang, T.D. Waite, Recent advances in Cu-Fenton systems for the treatment of industrial wastewaters: Role of Cu complexes and Cu composites, J. Hazard. Mater. 392 (2020) 122261. https://doi.org/10.1016/j.jhazmat.2020.122261.
[19] S. Guo, M. Chen, L. You, Y. Wei, C. Cai, Q. Wei, H. Zhang, K. Zhou, 3D printed hierarchically porous zero-valent copper for efficient pollutant degradation through peroxymonosulfate activation, Sep. Purif. Technol. 305 (2023) 122437. https://doi.org/10.1016/j.seppur.2022.122437.
[20] Y. Li, J. Wang, Z. Wei, W. Li, W. Duan, X. Feng, Q. Ma, Q. Zhang, H. Chen, X. Wu, Effective periodate activation by peculiar Cu2O nanocrystal for antibiotics degradation: The critical role of structure and underlying mechanism study, Appl. Catal. B Environ. 341 (2024) 123351. https://doi.org/10.1016/j.apcatb.2023.123351.
[21] A. Fiorentino, R. Cucciniello, A. Di Cesare, D. Fontaneto, P. Prete, L. Rizzo, G. Corno, A. Proto, Disinfection of urban wastewater by a new photo-Fenton like process using Cu-iminodisuccinic acid complex as catalyst at neutral pH, Water Res. 146 (2018) 206–215. https://doi.org/10.1016/j.watres.2018.08.024.
[22] Y. Fang, D. Luan, X.W. (David) Lou, Recent Advances on Mixed Metal Sulfides for Advanced Sodium-Ion Batteries, Adv. Mater. 32 (2020) 2002976. https://doi.org/10.1002/adma.202002976.
[23] Y. Huang, L. Nengzi, X. Zhang, J. Gou, Y. Gao, G. Zhu, Q. Cheng, X. Cheng, Catalytic degradation of ciprofloxacin by magnetic CuS/Fe2O3/Mn2O3 nanocomposite activated peroxymonosulfate: Influence factors, degradation pathways and reaction mechanism, Chem. Eng. J. 388 (2020) 124274. https://doi.org/10.1016/j.cej.2020.124274.
[24] B. Mao, Q. An, B. Zhai, Z. Xiao, S. Zhai, Multifunctional hollow polydopamine-based composites (Fe3O4/PDA@Ag) for efficient degradation of organic dyes, RSC Adv. 6 (2016) 47761–47770. https://doi.org/10.1039/C6RA05954F.
[25] S. Cheng, X. Pan, C. Zhang, X. Lin, Q. Zhuang, Y. Jiao, W. Dong, X. Qi, UV-assisted ultrafast construction of robust Fe3O4/polydopamine/Ag Fenton-like catalysts for highly efficient micropollutant decomposition, Sci. Total Environ. 810 (2022) 151182. https://doi.org/10.1016/j.scitotenv.2021.151182.
[26] B. Jin, D. Zhao, H. Yu, W. Liu, C. Zhang, M. Wu, Rapid degradation of organic pollutants by Fe3O4@PDA/Ag catalyst in advanced oxidation process, Chemosphere 307 (2022) 135791. https://doi.org/10.1016/j.chemosphere.2022.135791.
[27] Q.U. Ain, U. Rasheed, M. Yaseen, H. Zhang, Z. Tong, Superior dye degradation and adsorption capability of polydopamine modified Fe3O4-pillared bentonite composite, J. Hazard. Mater. 397 (2020) 122758. https://doi.org/10.1016/j.jhazmat.2020.122758.
[28] W. Chen, T. Zhou, D. Gu, Y. He, Z. Zhang, J. Tian, F. Fu, Polydopamine-coated carbonized cotton fabrics with β-FeOOH nanorods composites for highly efficient photo-Fenton degradation of organic

pollutants, Appl. Surf. Sci. 637 (2023) 157955. https://doi.org/10.1016/j.apsusc.2023.157955.
[29] Concerted catalytic and photocatalytic degradation of organic pollutants over CuS/g-C3N4 catalysts under light and dark conditions, J. Adv. Res. 16 (2019) 135–143. https://doi.org/10.1016/j.jare.2018.10.003.
[30] Z. Huang, L. Wang, H. Wu, H. Hu, H. Lin, L. Qin, Q. Li, Shape-controlled synthesis of CuS as a Fenton-like photocatalyst with high catalytic performance and stability, J. Alloys Compd. 896 (2022) 163045. https://doi.org/10.1016/j.jallcom.2021.163045.
[31] T. Zhang, Y. Xiang, Y. Su, Y. Zhang, X. Huang, X. Qian, Anchoring of copper sulfide on cellulose fibers with polydopamine for efficient and recyclable photocatalytic degradation of organic dyes, Ind. Crops Prod. 187 (2022) 115357. https://doi.org/10.1016/j.indcrop.2022.115357.
[32] M. Saranya, C. Santhosh, R. Ramachandran, P. Kollu, P. Saravanan, M. Vinoba, S.K. Jeong, A.N. Grace, Hydrothermal growth of CuS nanostructures and its photocatalytic properties, Powder Technol. 252 (2014) 25–32. https://doi.org/10.1016/j.powtec.2013.10.031.
[33] H. Wu, V. W. Or, S. Gonzalez-Calzada, V. H. Grassian, CuS nanoparticles in humid environments: adsorbed water enhances the transformation of CuS to CuSO 4, Nanoscale 12 (2020) 19350–19358. https://doi.org/10.1039/D0NR05934J.
[34] Fabrication of h-BN-rGO@PDA nanohybrids for composite coatings with enhanced anticorrosion performance, Prog. Org. Coat. 130 (2019) 124–131. https://doi.org/10.1016/j.porgcoat.2019.01.059.
[35] L. Shang, W. Li, X. Wang, L. Ma, L. Li, Q. Duan, Y. Li, Preparation of magnetic Fe3O4@PDA/CuS core-shell nanocomposite as a green photocatalyst, Synth. Met. 292 (2023) 117230. https://doi.org/10.1016/j.synthmet.2022.117230.
[36] X. Wang, C. Deng, Preparation of magnetic graphene @polydopamine @Zr-MOF material for the extraction and analysis of bisphenols in water samples, Talanta 144 (2015) 1329–1335. https://doi.org/10.1016/j.talanta.2015.08.014.
[37] K. Zhang, J. Zhang, A. Yang, Photoheating Effects of CuS@PEI_GQDs Nanoshells under Near-Infrared Laser and Sunlight Irradiation, Cryst. Growth Des. 23 (2023) 1697–1708. https://doi.org/10.1021/acs.cgd.2c01274.
[38] Preparation of photothermal alginate/chitosan derivative/CuS@polydopamine composite fibers and application in desalination, Int. J. Biol. Macromol. 277 (2024) 134142. https://doi.org/10.1016/j.ijbiomac.2024.134142.
[39] H. Zhang, C. Zhou, H. Zeng, H. Wu, L. Yang, L. Deng, Z. Shi, ZIF-8 assisted synthesis of magnetic core–shell FeO@CuS nanoparticles for efficient sulfadiazine degradation via HO activation: Performance and mechanism3422, J. Colloid Interface Sci. 594 (2021) 502–512. https://doi.org/10.1016/j.jcis.2021.03.057.
[40] J. Zhang, H. Zeng, L. Bu, S. Zhou, Z. Shi, L. Deng, Cu0 incorporated cobalt/nitrogen doped carbonaceous frameworks derived from ZIF-67 (Cu@CoNC) as PMS activator for efficient degradation of naproxen: Direct electron transfer and 1O2 dominated nonradical mechanisms, Chem. Eng. J. 454 (2023) 139989. https://doi.org/10.1016/j.cej.2022.139989.
[41] X. Xie, Y. Hu, H. Cheng, Rapid degradation of p-arsanilic acid with simultaneous arsenic removal from aqueous solution using Fenton process, Water Res. 89 (2016) 59–67. https://doi.org/10.1016/j.watres.2015.11.037.
[42] Y.-Y. Chen, Y.-L. Ma, J. Yang, L.-Q. Wang, J.-M. Lv, C.-J. Ren, Aqueous tetracycline degradation by H2O2 alone: Removal and transformation pathway, Chem. Eng. J. 307 (2017) 15–23. https://doi.org/10.1016/j.cej.2016.08.046.

[43] F. Bernsmann, B. Frisch, C. Ringwald, V. Ball, Protein adsorption on dopamine–melanin films: Role of electrostatic interactions inferred from ζ-potential measurements versus chemisorption, J. Colloid Interface Sci. 344 (2010) 54–60. https://doi.org/10.1016/j.jcis.2009.12.052.
[44] R. Tejido-Rastrilla, S. Ferraris, W.H. Goldmann, A. Grünewald, R. Detsch, G. Baldi, S. Spriano, A.R. Boccaccini, Studies on Cell Compatibility, Antibacterial Behavior, and Zeta Potential of Ag-Containing Polydopamine-Coated Bioactive Glass-Ceramic, Materials 12 (2019) 500. https://doi.org/10.3390/ma12030500.
[45] J.E. Grebel, J.J. Pignatello, W.A. Mitch, Effect of Halide Ions and Carbonates on Organic Contaminant Degradation by Hydroxyl Radical-Based Advanced Oxidation Processes in Saline Waters, Environ. Sci. Technol. 44 (2010) 6822–6828. https://doi.org/10.1021/es1010225.
[46] H. Liang, X. Li, Y. Yang, K. Sze, Effects of dissolved oxygen, pH, and anions on the 2,3-dichlorophenol degradation by photocatalytic reaction with anodic TiO2 nanotube films, Chemosphere 73 (2008) 805–812. https://doi.org/10.1016/j.chemosphere.2008.06.007.
[47] A. Jawad, X. Lu, Z. Chen, G. Yin, Degradation of Chlorophenols by Supported Co–Mg–Al Layered Double Hydrotalcite with Bicarbonate Activated Hydrogen Peroxide, J. Phys. Chem. A 118 (2014) 10028–10035. https://doi.org/10.1021/jp5085313.
[48] Y. Zhang, J. Lou, L. Wu, M. Nie, C. Yan, M. Ding, P. Wang, H. Zhang, Minute Cu coupling with HCO for efficient degradation of acetaminophen via HO activation2+3−22, Ecotoxicol. Environ. Saf. 221 (2021) 112422. https://doi.org/10.1016/j.ecoenv.2021.112422.
[49] H. Zeng, L. Deng, H. Zhang, C. Zhou, Z. Shi, Development of oxygen vacancies enriched CoAl hydroxide@hydroxysulfide hollow flowers for peroxymonosulfate activation: A highly efficient singlet oxygen-dominated oxidation process for sulfamethoxazole degradation, J. Hazard. Mater. 400 (2020) 123297. https://doi.org/10.1016/j.jhazmat.2020.123297.
[50] T. Peng, H. Zhang, S. Xia, S. Zhou, Z. Shi, G. Li, L. Deng, MoS2 Nanosheets Anchored onto MIL-100(Fe)-Derived FeS2 as a Peroxymonosulfate Activator for Efficient Sulfamethoxazole Degradation: Insights into the Mechanism, ACS EST Water 3 (2023) 213–226. https://doi.org/10.1021/acsestwater.2c00501.
[51] X. Liu, P. Xu, Q. Fu, R. Li, C. He, W. Yao, L. Wang, S. Xie, Z. Xie, Q. He, J.C. Crittenden, Ferric ion promoted degradation of acetaminophen with zero − valent copper activated peroxymonosulfate process, Chem. Eng. J. 426 (2021) 131679. https://doi.org/10.1016/j.cej.2021.131679.
[52] F. Sun, T. Chen, Z. Chu, P. Zhai, H. Liu, Q. Wang, X. Zou, D. Chen, The synergistic effect of calcite and Cu2+ on the degradation of sulfadiazine via PDS activation: A role of Cu(lll), Water Res. 219 (2022) 118529. https://doi.org/10.1016/j.watres.2022.118529.
[53] Y. Wei, J. Miao, J. Ge, J. Lang, C. Yu, L. Zhang, P.J.J. Alvarez, M. Long, Ultrahigh Peroxymonosulfate Utilization Efficiency over CuO Nanosheets via Heterogeneous Cu(III) Formation and Preferential Electron Transfer during Degradation of Phenols, Environ. Sci. Technol. 56 (2022) 8984–8992. https://doi.org/10.1021/acs.est.2c01968.
[54] X. Liu, M. Li, Z. Xie, P. Li, C. Du, Y. Su, Oxygen vacancy-enriched kaolinite/WO3-x nanocomposites exhibiting enhanced photo-synergetic H2O2 activation for tetracycline degradation boosted by hydroxyl groups and exciton, Sep. Purif. Technol. 347 (2024) 127675. https://doi.org/10.1016/j.seppur.2024.127675.
[55] X. Zhang, B. Yang, H. Quan, H. Pei, S.-Q. Guo, Surface methyl/methylene regulates WO directional activation of molecular oxygen into singlet oxygen for the removal of organic pollutants in

water3, Sep. Purif. Technol. 346 (2024) 127559. https://doi.org/10.1016/j.seppur.2024.127559.
[56] J. Miao, W. Geng, P.J.J. Alvarez, M. Long, 2D N-Doped Porous Carbon Derived from Polydopamine-Coated Graphitic Carbon Nitride for Efficient Nonradical Activation of Peroxymonosulfate, Environ. Sci. Technol. 54 (2020) 8473–8481. https://doi.org/10.1021/acs.est.0c03207.
[57] Y. Yu, J.G. Shapter, R. Popelka-Filcoff, J.W. Bennett, A.V. Ellis, Copper removal using bio-inspired polydopamine coated natural zeolites, J. Hazard. Mater. 273 (2014) 174–182. https://doi.org/10.1016/j.jhazmat.2014.03.048.
[58] M. Cheng, Y. Liu, D. Huang, C. Lai, G. Zeng, J. Huang, Z. Liu, C. Zhang, C. Zhou, L. Qin, W. Xiong, H. Yi, Y. Yang, Prussian blue analogue derived magnetic Cu-Fe oxide as a recyclable photo-Fenton catalyst for the efficient removal of sulfamethazine at near neutral pH values, Chem. Eng. J. 362 (2019) 865–876. https://doi.org/10.1016/j.cej.2019.01.101.
[59] J. Peng, X. Lu, X. Jiang, Y. Zhang, Q. Chen, B. Lai, G. Yao, Degradation of atrazine by persulfate activation with copper sulfide (CuS): Kinetics study, degradation pathways and mechanism, Chem. Eng. J. 354 (2018) 740–752. https://doi.org/10.1016/j.cej.2018.08.038.
[60] S.-Q. Zhang, X. Liu, Q.-X. Sun, O. Johnson, T. Yang, M.-L. Chen, J.-H. Wang, W. Chen, CuS@PDA–FA nanocomposites: a dual stimuli-responsive DOX delivery vehicle with ultrahigh loading level for synergistic photothermal–chemotherapies on breast cancer, J. Mater. Chem. B 8 (2020) 1396–1404. https://doi.org/10.1039/C9TB02440A.
[61] Can Cu2ZnSnS4 nanoparticles be used as heterogeneous catalysts for sulfadiazine degradation?, J. Hazard. Mater. 395 (2020) 122613. https://doi.org/10.1016/j.jhazmat.2020.122613.
[62] H. Zhang, L. Deng, J. Chen, Y. Zhang, M. Liu, Y. Han, Y. Chen, H. Zeng, Z. Shi, How MoS2 assisted sulfur vacancies featured Cu2S in hollow Cu2S@MoS2 nanoboxes to activate H2O2 for efficient sulfadiazine degradation?, Chem. Eng. J. 446 (2022) 137364. https://doi.org/10.1016/j.cej.2022.137364.
[63] S. Dolai, R. Dey, S. Das, S. Hussain, R. Bhar, A.K. Pal, Cupric oxide (CuO) thin films prepared by reactive d.c. magnetron sputtering technique for photovoltaic application, J. Alloys Compd. 724 (2017) 456–464. https://doi.org/10.1016/j.jallcom.2017.07.061.
[64] M. Cheng, Y. Liu, D. Huang, C. Lai, G. Zeng, J. Huang, Z. Liu, C. Zhang, C. Zhou, L. Qin, W. Xiong, H. Yi, Y. Yang, Prussian blue analogue derived magnetic Cu-Fe oxide as a recyclable photo-Fenton catalyst for the efficient removal of sulfamethazine at near neutral pH values, Chem. Eng. J. 362 (2019) 865–876. https://doi.org/10.1016/j.cej.2019.01.101.
[65] Z. Yang, J. Qian, A. Yu, B. Pan, Singlet oxygen mediated iron-based Fenton-like catalysis under nanoconfinement, Proc. Natl. Acad. Sci. 116 (2019) 6659–6664. https://doi.org/10.1073/pnas.1819382116.
[66] A.U. Khan, M. Kasha, Singlet molecular oxygen in the Haber-Weiss reaction., Proc. Natl. Acad. Sci. 91 (1994) 12365–12367. https://doi.org/10.1073/pnas.91.26.12365.
[67] B. Sheng, C. Deng, Y. Li, S. Xie, Z. Wang, H. Sheng, J. Zhao, In Situ Hydroxylation of a Single-Atom Iron Catalyst for Preferential 1O2 Production from H2O2, ACS Catal. 12 (2022) 14679–14688. https://doi.org/10.1021/acscatal.2c04484.
[68] F. Xu, C. Lai, M. Zhang, B. Li, L. Li, S. Liu, D. Ma, X. Zhou, H. Yan, X. Huo, B. Wang, H. Yi, L. Qin, L. Tang, High-loaded single-atom Cu-N3 sites catalyze hydrogen peroxide decomposition to selectively induce singlet oxygen production for wastewater purification, Appl. Catal. B Environ. 339 (2023) 123075. https://doi.org/10.1016/j.apcatb.2023.123075.
[69] Efficient degradation of tetracycline by heterogeneous electro-Fenton process using Cu-doped

Fe@Fe2O3: Mechanism and degradation pathway, Chem. Eng. J. 382 (2020) 122970. https://doi.org/10.1016/j.cej.2019.122970.
[70] Z. Yin, Y. Liu, S. Zhou, Z. Yang, W. Yang, Constructing zirconium based metal–organic frameworks based electrically-driven self-cleaning membrane for removal of tetracycline: Effect of ligand substitution, Chem. Eng. J. 450 (2022) 138100. https://doi.org/10.1016/j.cej.2022.138100.
[71] X. Li, T. Hou, L. Yan, L. Shan, X. Meng, Y. Zhao, Efficient degradation of tetracycline by CoFeLa-layered double hydroxides catalyzed peroxymonosulfate: Synergistic effect of radical and nonradical pathways, J. Hazard. Mater. 398 (2020) 122884. https://doi.org/10.1016/j.jhazmat.2020.122884.
[72] M. Jiang, X. Wang, R. Han, P. Ning, I. Lynch, J. Ma, Establishing photocatalysis-self-Fenton system over a S-scheme Fe/Fe2O3@CuBi2O4 for enhancing TC removal via in-situ generating H2O2 and Fe/Cu dual-metal electron cycle: Radical and non-radical pathways, Sep. Purif. Technol. 354 (2025) 128675. https://doi.org/10.1016/j.seppur.2024.128675.
[73] X. Li, Y. Jia, J. Zhang, Y. Qin, Y. Wu, M. Zhou, J. Sun, Efficient removal of tetracycline by H2O2 activated with iron-doped biochar: Performance, mechanism, and degradation pathways, Chin. Chem. Lett. 33 (2022) 2105–2110. https://doi.org/10.1016/j.cclet.2021.08.054.
[74] M. Nie, Y. Li, L. Li, J. He, P. Hong, K. Zhang, X. Cai, L. Kong, J. Liu, Ultrathin iron-cobalt oxide nanosheets with enhanced H2O2 activation performance for efficient degradation of tetracycline, Appl. Surf. Sci. 535 (2021) 147655. https://doi.org/10.1016/j.apsusc.2020.147655.
[75] S. Yang, Y. Feng, D. Gao, X. Wang, N. Suo, Y. Yu, S. Zhang, Electrocatalysis degradation of tetracycline in a three-dimensional aeration electrocatalysis reactor (3D-AER) with a flotation-tailings particle electrode (FPE): Physicochemical properties, influencing factors and the degradation mechanism, J. Hazard. Mater. 407 (2021) 124361. https://doi.org/10.1016/j.jhazmat.2020.124361.
[76] Z. Li, C. Guo, J. Lyu, Z. Hu, M. Ge, Tetracycline degradation by persulfate activated with magnetic Cu/CuFe2O4 composite: Efficiency, stability, mechanism and degradation pathway, J. Hazard. Mater. 373 (2019) 85–96. https://doi.org/10.1016/j.jhazmat.2019.03.075.
[77] D. Chen, Q. Bai, T. Ma, X. Jing, Y. Tian, R. Zhao, G. Zhu, Stable metal–organic framework fixing within zeolite beads for effectively static and continuous flow degradation of tetracycline by peroxymonosulfate activation, Chem. Eng. J. 435 (2022) 134916. https://doi.org/10.1016/j.cej.2022.134916.

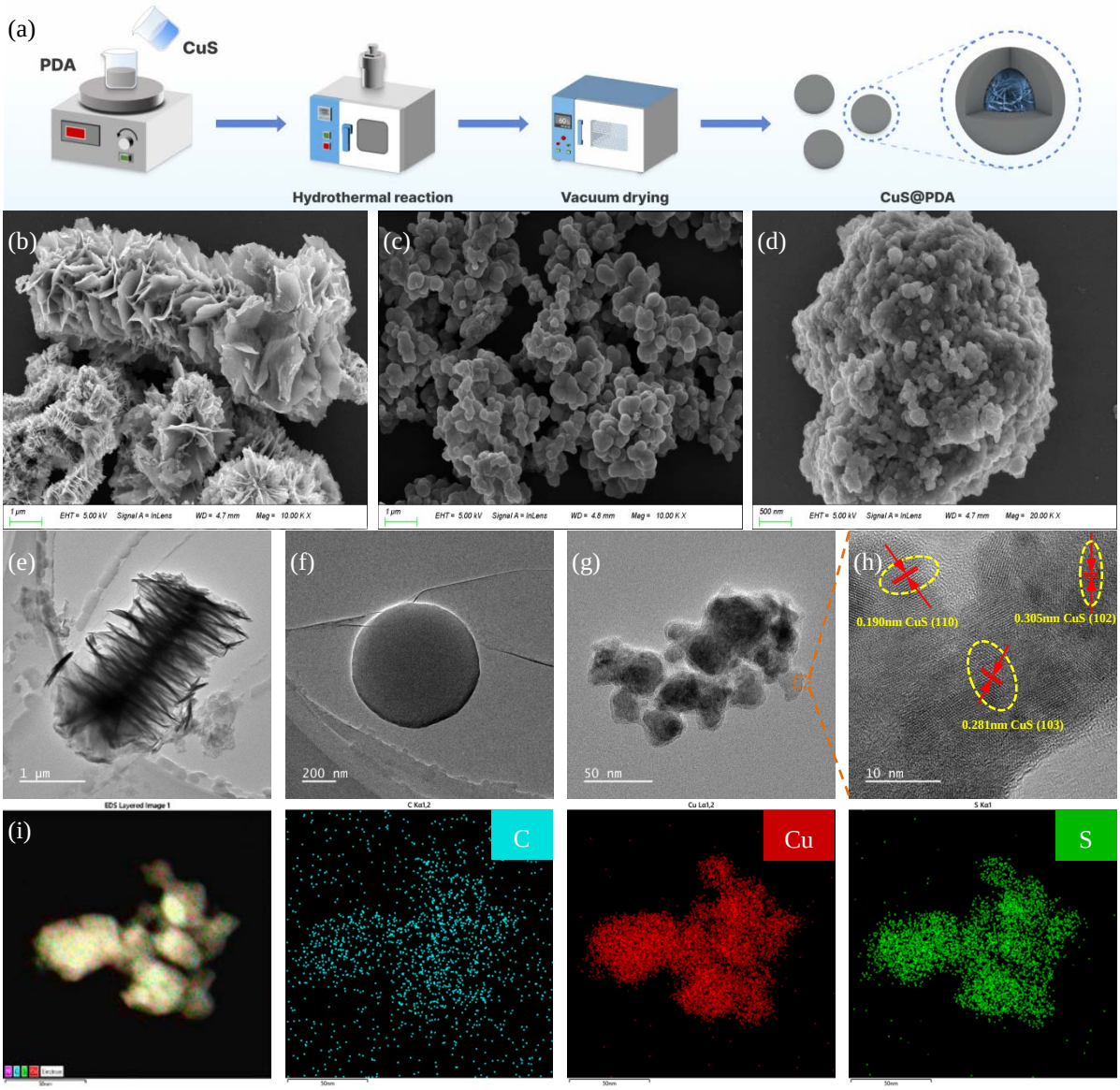

Figure 1. (a) The schematic synthesis route of CuS@PDA; SEM images of (b) CuS, (c) PDA and (d) CuS@PDA; TEM images of (e) CuS, (f) PDA and (g, h) CuS@PDA; (i) EDX elemental mapping images of CuS@PDA.

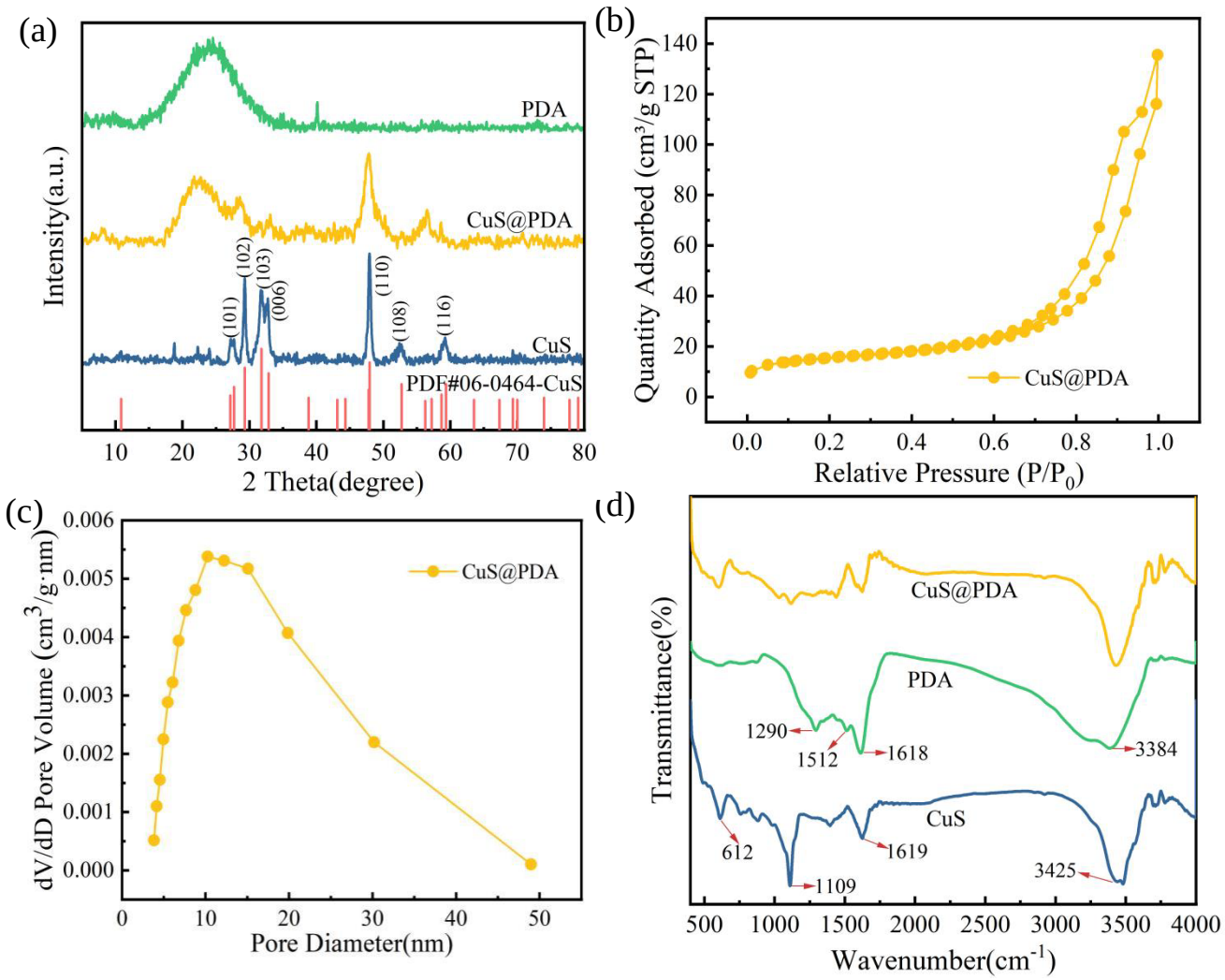

Figure 2. (a) XRD patterns of CuS, PDA and CuS@PDA; (b) N_2 adsorption/desorption isotherm and (c) pore size distribution of CuS@PDA; (d) FTIR spectra of CuS, PDA and CuS@PDA.

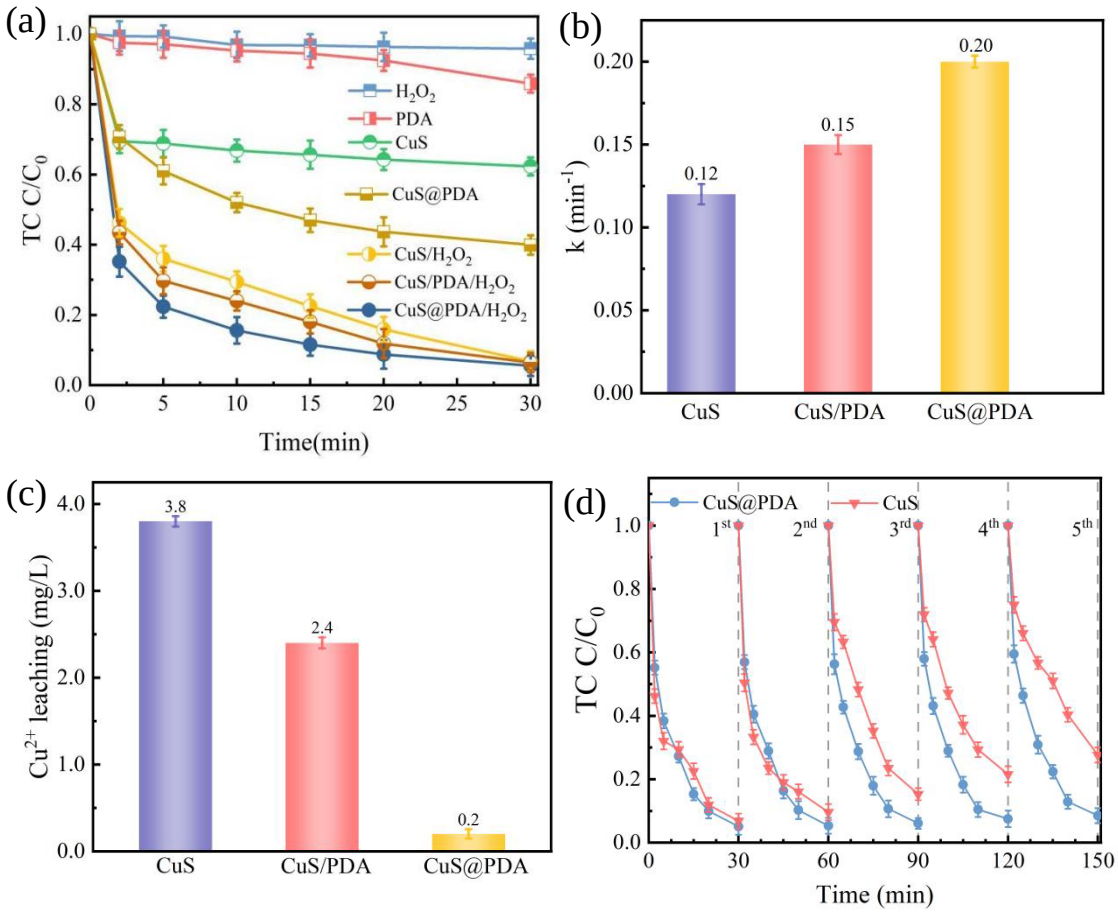

Figure 3. (a) TC removal in different systems; (b) the fitted kinetic rate constants of TC degradation by CuS, CuS/PDA, and CuS@PDA in the presence of H_2O_2; (c) Cu^{2+} leakage from different catalysts; (d) recyclability of CuS and CuS@PDA for activating H_2O_2 to degrade TC ([TC] = 40 μM, [catalyst] = 0.1 g/L, [H_2O_2] = 5 mM).

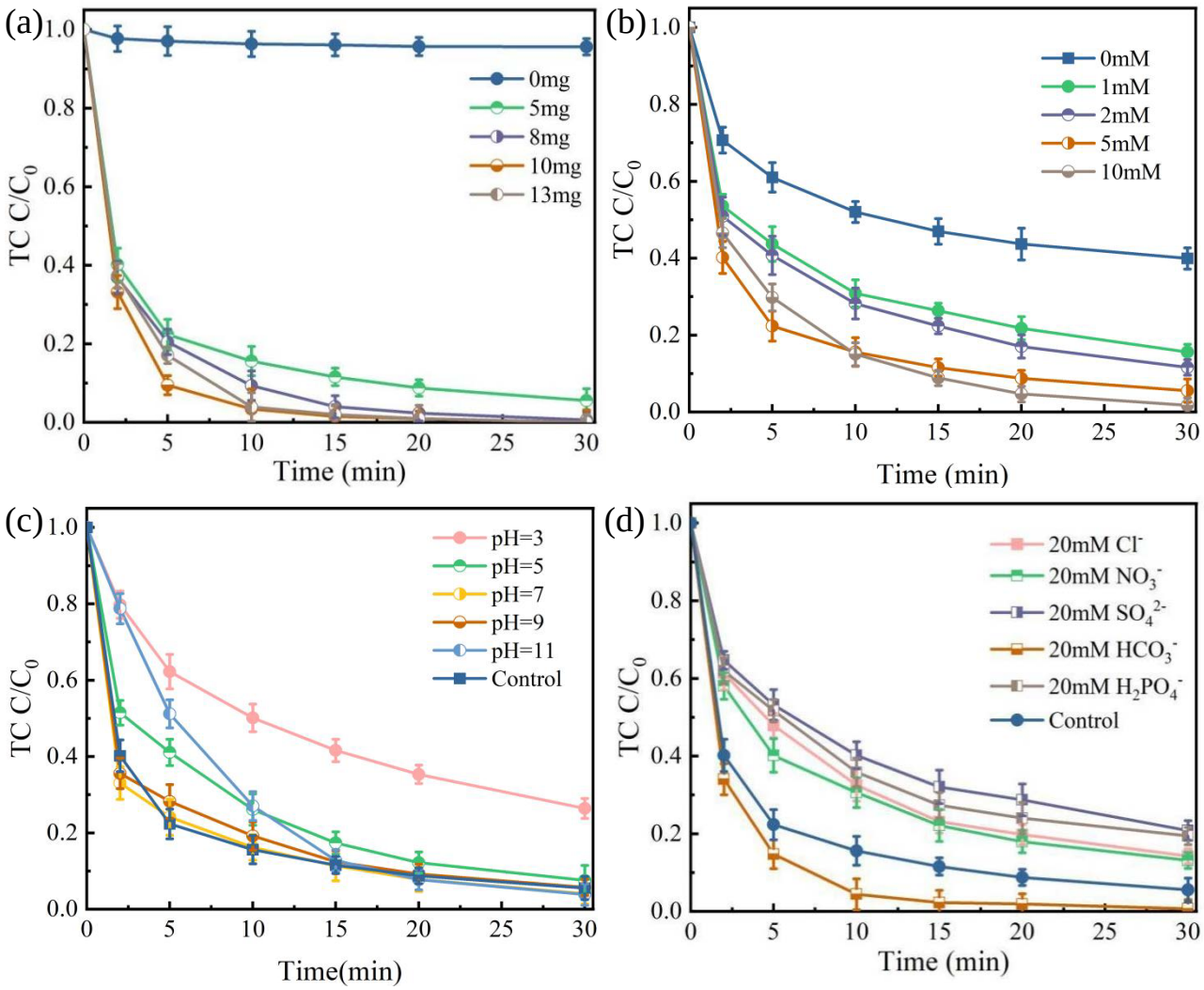

Figure 4. Influences of (a) catalyst dosage, (b) H_2O_2 concentration, (c) initial solution pH, and (d) coexisting ions on TC degradation ([catalyst] = 0.1 g/L (except a), [H_2O_2] = 5 mM (except b), [TC] = 40 μM).

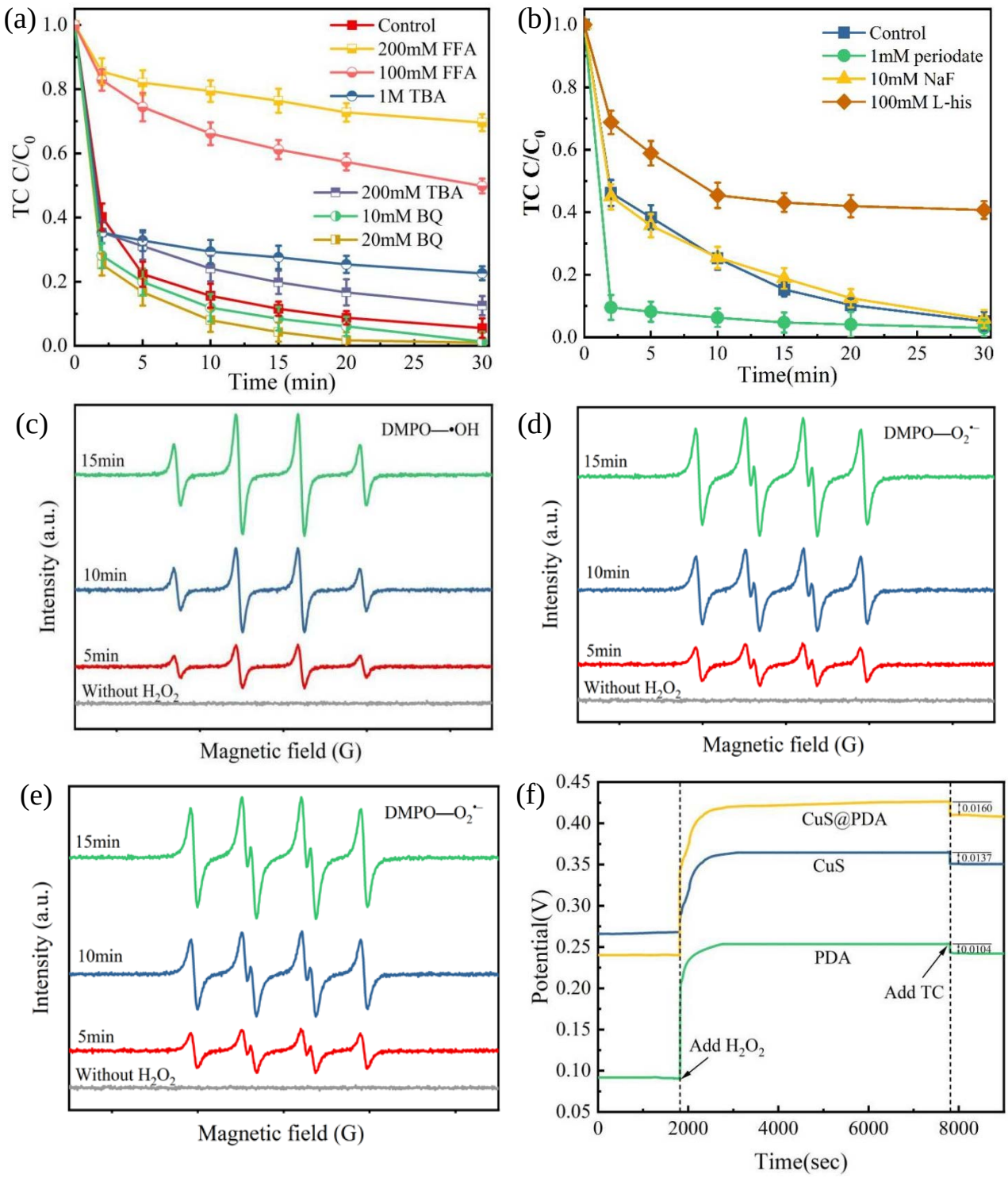

Figure 5. Effect of different radical scavengers (a), periodate, NaF and L-his (b) on the degradation of TC; EPR spectroscopy of (c) DMPO-•OH, (d) DMPO- $O_2^{\bullet-}$ and (e) TEMP-$^1O_2$; (f) open circuit potential contrast of working electrodes in different systems ([TC] = 40μM, [catalyst] = 0.1g/L, [H_2O_2] = 5 mM).

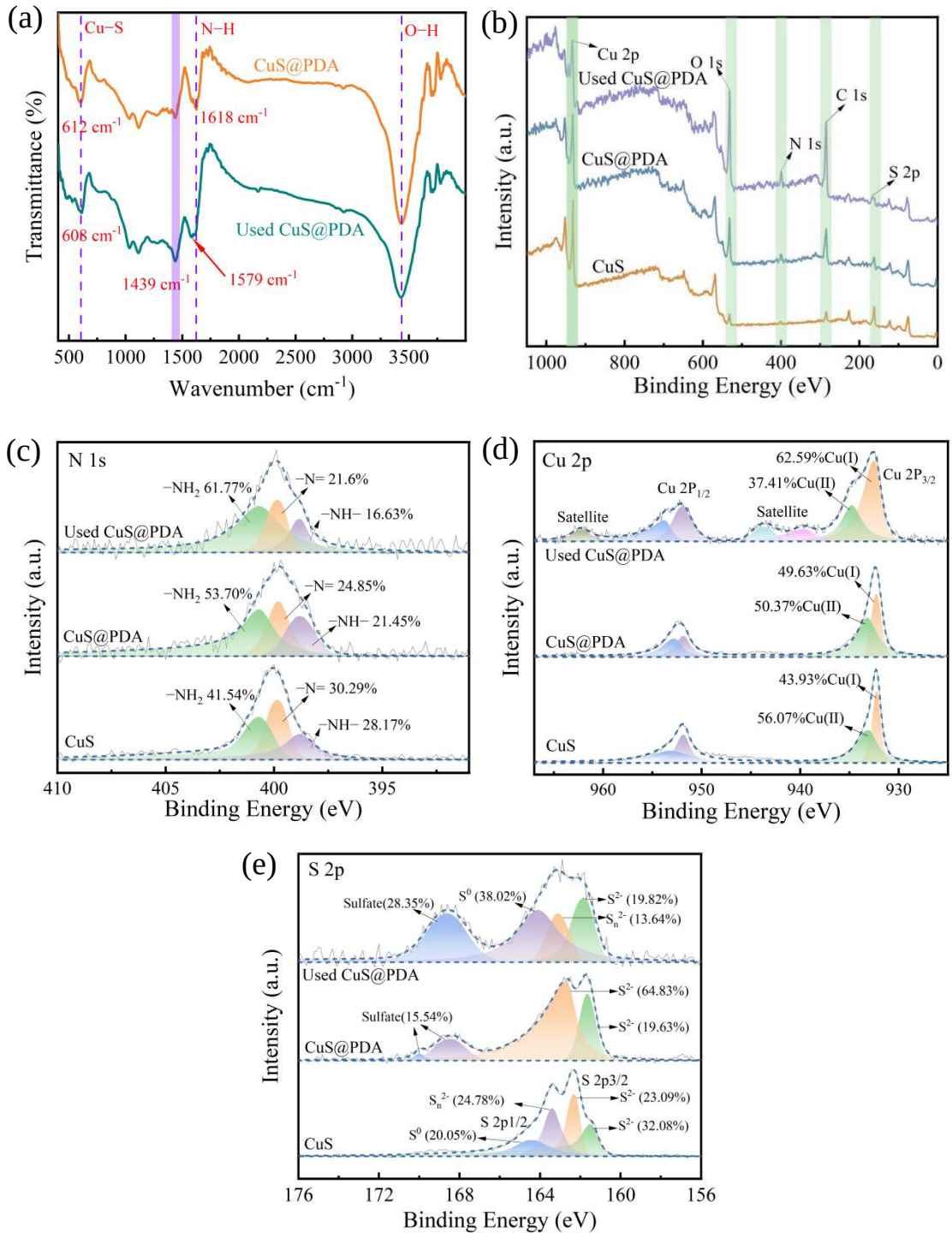

Figure 6. The FTIR spectrum of the fresh and used CuS@PDA; The XPS spectrum of CuS, CuS@PDA and used CuS@PDA: (a) survey, (b) N 1s, (c) Cu 2p, and (d) S 2p.

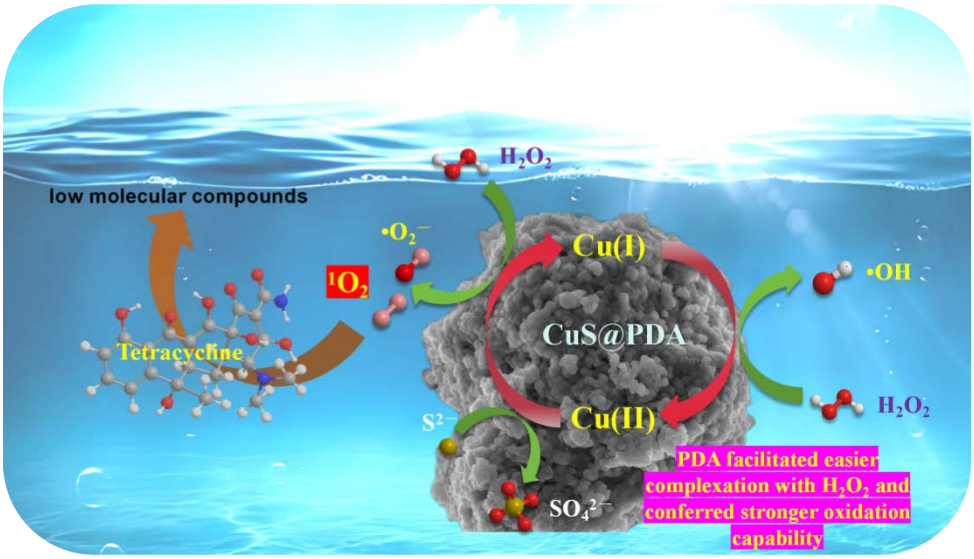

Figure 7. Schematically illustrating the degradation mechanisms of TC by CuS@PDA/H_2O_2.

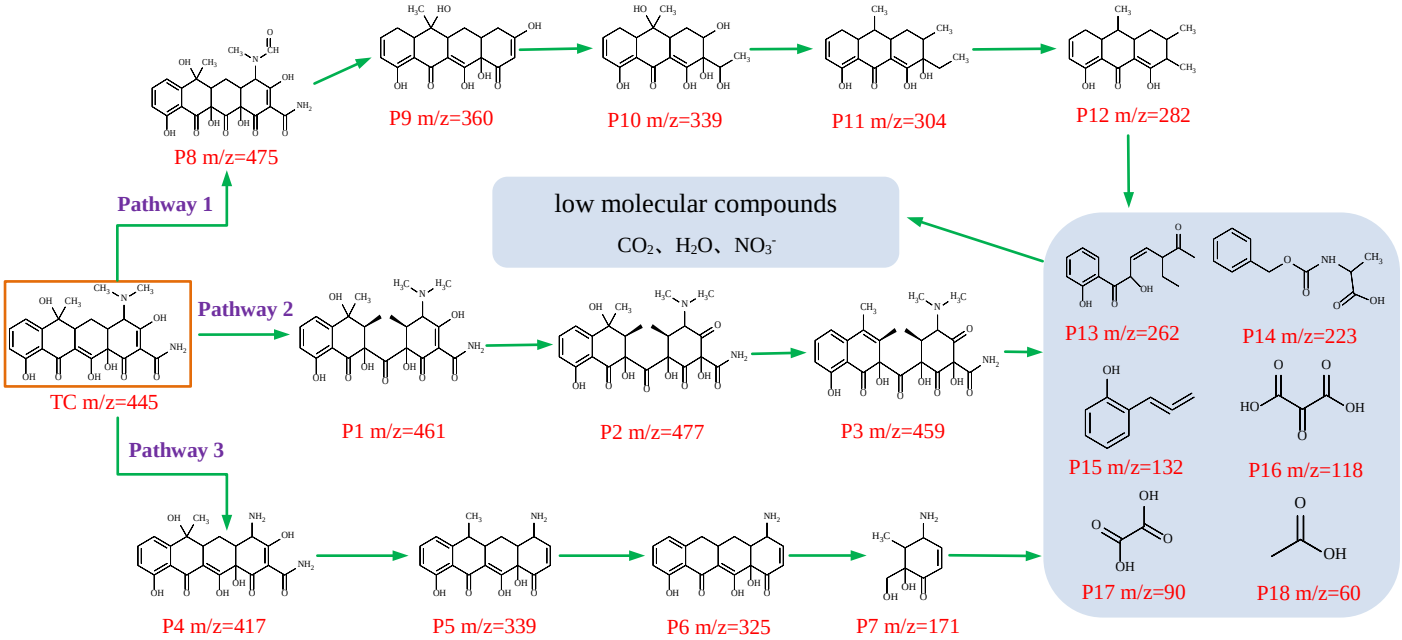

Figure 8. Possible degradation pathways of TC by CuS@PDA/H_2O_2 system.

Supporting information

for

A novel polydopamine-loaded copper sulfide (CuS@PDA) for activating H_2O_2 to eliminate tetracycline via $^1O_2$ dominated oxidation pathway

Zhou Shi[a], Chenxi He[a], Hao Huang[a], Xile Huang[a], Tong Hu[a], Yijia He[a], Dazhi Yang[a], Simeng Xia[a,*], Haojie Zhang[a,b,*], Lin Deng[a,*]

a. Hunan Engineering Research Center of Water Security Technology and Application, College of Civil Engineering, Hunan University, Changsha 410082, China

b. Helmholtz Centre for Environmental Research-UFZ, Department of Technical Biogeochemistry, Leipzig 04318, Germany

*Corresponding authors.

E-mail addresses: symeon@hnu.edu.cn (S. Xia); haojie.zhang@ufz.de (H. Zhang); lindeng@hnu.edu.cn (L. Deng)

Number of pages: 15
Number of text: 1
Number of tables: 3
Number of figures: 4

Text S1. Analytical and characterization methods

The surface morphology of the materials was characterized by a scanning electron microscope (SEM, ZEISS Sigma 300) with 3.0 kV scanning voltage and transmission electron microscopy (TEM, JEM F200). The crystal properties were determined by X-ray diffraction (XRD, Rigaku SmartLab SE) with r Cu-Kα adiation source (λ=0.154 nm, 40 kV, 40 mA) at a scan rate of 5 °/min. The Zetasizer Nano ZS (Malvern Instruments) was used to measure the Zeta potential of the samples. X-ray photoelectron spectroscopy (XPS) was applied to identify the elemental composition and chemical states using AXIS SUPRA+ equipped with an Al Kα X-ray source. ROS was recognized by Electron paramagnetic resonance (EPR) with a Bruker A-300 spectrometer using 5,5-Dimethyl-1-pyrroline-N-oxide (DMPO) and 2,2,6,6-tetramethyl-4-piperidone (TEMP) as spin- trapping agents.

The concentration of TC was determined by high-performance liquid chromatography (HPLC, Agilent 1260, USA) equipped with a Symmetry C18 column (150mm×4.6mm×5μm, Agilent, USA) and a VWD detector (Agilent, USA). For TC determination, the wavelength of the detector was 365 nm, the temperature of C18 column was maintained at 25 ℃, the mobile phase consisted of 50% methanol and 50% acetic acid with a flow rate of 1.0 mL/min. Concentrations of the other contaminants SMX, CBZ, CM and SDZ were also determined by high performance liquid chromatography (HPLC, Agilent 1260, USA). The HPLC analysis conditions for various organic compounds are shown in Table S1. The concentration of H_2O_2 in solution was measured by a photometric method on an UV-vis spectrometer (HITACHI,

U3900, Japan) at 415 nm using Titanium sulfate as chromogenic reagent. Graphite furnace atomizer (GFA-6880, Shimadzu) Atomic Absorption Spectrophotometry (AA-6880, Shimadzu) was used to detect the metal ions content.

Table S1. HPLC analysis conditions for various organic compounds.

Target pollutants	Flow rate (ml/min)	Temperature (°C)	Wavelength (nm)	Water (% v/v)	Acetonitrile (% v/v)	Methanol (% v/v)
Sulfadiazine (SDZ)	1	25	290	70	0	30
Sulfamethoxazole (SMX)	1	30	269	75[a]	25	0
Carbamazepine (CBZ)	1	30	280	30	0	70
Coumarin (CM)	1	35	274	20	0	80

Water[a]: 0.1% acetic acid;

Table S2. Comparison of kinetic rate constants of TC degradation by different catalysts in H_2O_2-based AOPs.

Catalyst	Dosage	Oxidant	Pollutant	pH	k (min^{-1})	Ref.
Fe-BC	0.2 g/L	H_2O_2, 1 mM	TC, 20 mg/L	3.0	0.1550	[S1]
FeOCl	0.35 mg/L	H_2O_2, 5 mM	TC, 60 mg/L	4.0	0.0034	[S2]
CoFe-ONSs	0.3 g/L	H_2O_2, 20 mM	TC, 50 mg/L	7.0	0.055	[S3]
MgNCN/MgO (Pre2:1)	0.10 g/L	H_2O_2, 17.6 mM	TC, 50 mg/L	6.0	0.1245	[S4]
Fe-MOFs	0.15 g/L	H_2O_2, 10 mL/L	TC, 50 mg/L	4.1	0.0822	[S5]
C/CFO@A/C-0.25C-500	0.2 g/L	H_2O_2, 9.7 mM	TC, 15 mg/L	6.5	0.0212	[S6]
CQDs/α-FeOOH	0.25 g/L	H_2O_2, 0.5 mM	TC, 20mg/L	6.8	0.1525	[S7]
$CuFeS_2$	0.30 g/L	H_2O_2, 0.8 mM	TC, 50mg/L	5.1	0.0105	[S8]
CuS@PDA	0.10 g/L	H_2O_2, 5.0 mM	TC, 40 μM	7.1	**0.20**	This work

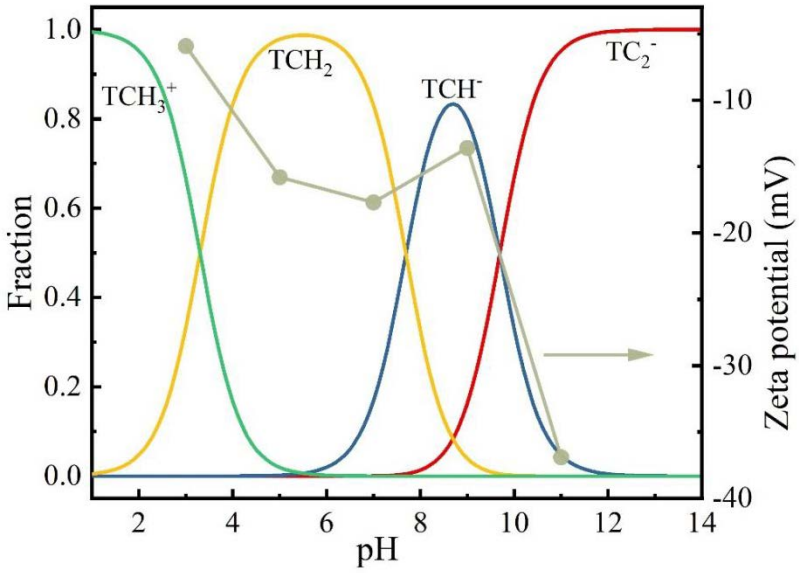

Figure S1. The speciation of TC and zeta potential of CuS@PDA.

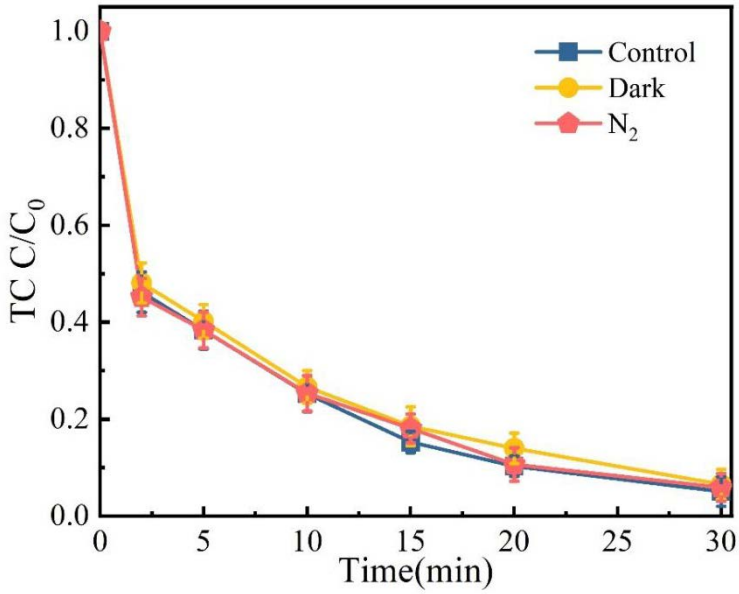

Figure S2. Effects of light irradiation and N_2 on the degradation of TC in CuS@PDA/H_2O_2 system. ([TC] = 40μM, [catalyst] = 0.1g/L, [H_2O_2] = 5 mM).

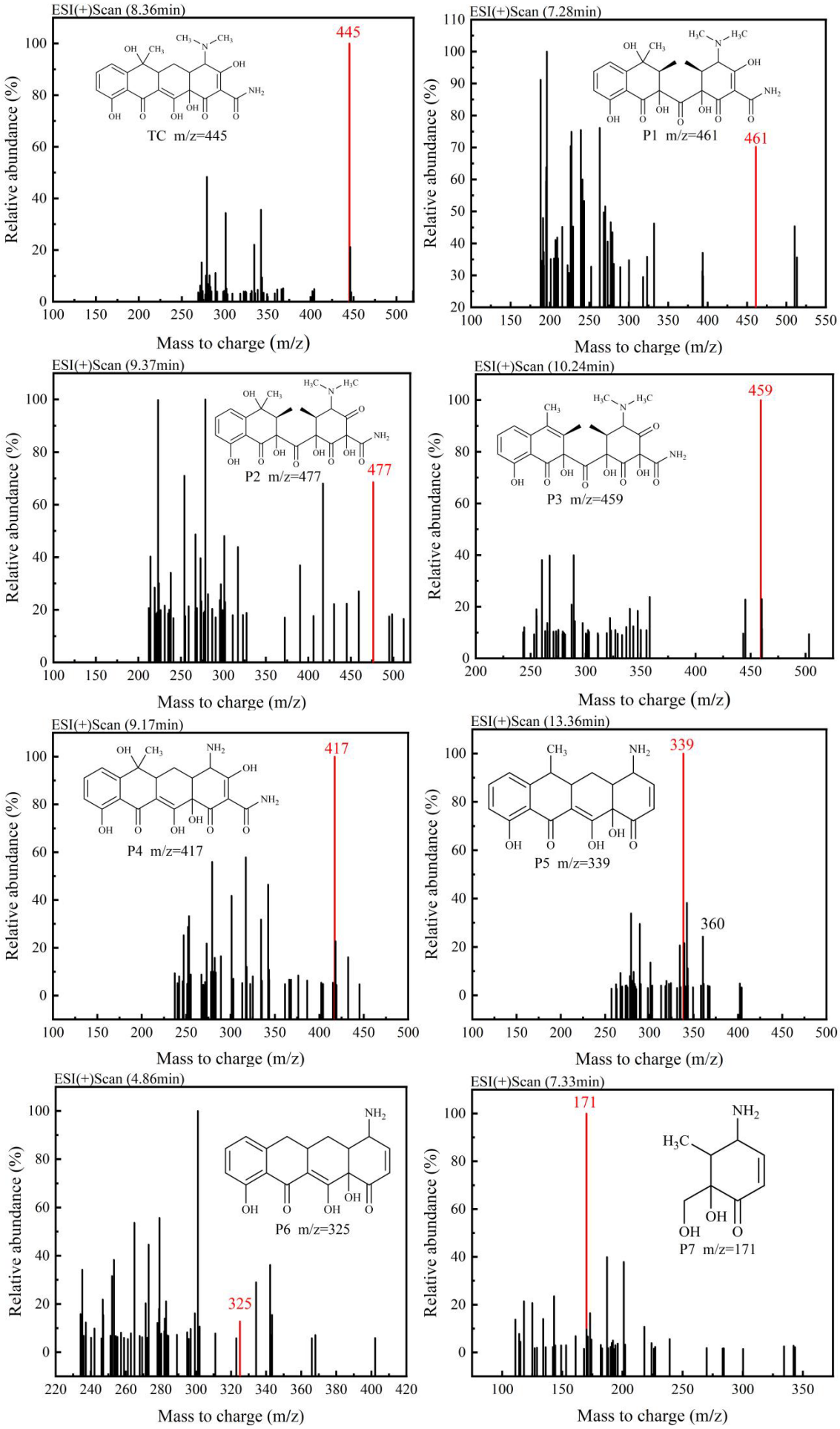
ESI(+)Scan (8.36min)
445
TC m/z=445
Relative abundance (%)
Mass to charge (m/z)
ESI(+)Scan (7.28min)
P1 m/z=461
461
Relative abundance (%)
Mass to charge (m/z)
ESI(+)Scan (9.37min)
P2 m/z=477
477
Relative abundance (%)
Mass to charge (m/z)
ESI(+)Scan (10.24min)
459
P3 m/z=459
Relative abundance (%)
Mass to charge (m/z)
ESI(+)Scan (9.17min)
417
P4 m/z=417
Relative abundance (%)
Mass to charge (m/z)
ESI(+)Scan (13.36min)
339
P5 m/z=339
360
Relative abundance (%)
Mass to charge (m/z)
ESI(+)Scan (4.86min)
P6 m/z=325
325
Relative abundance (%)
Mass to charge (m/z)
ESI(+)Scan (7.33min)
171
P7 m/z=171
Relative abundance (%)
Mass to charge (m/z)

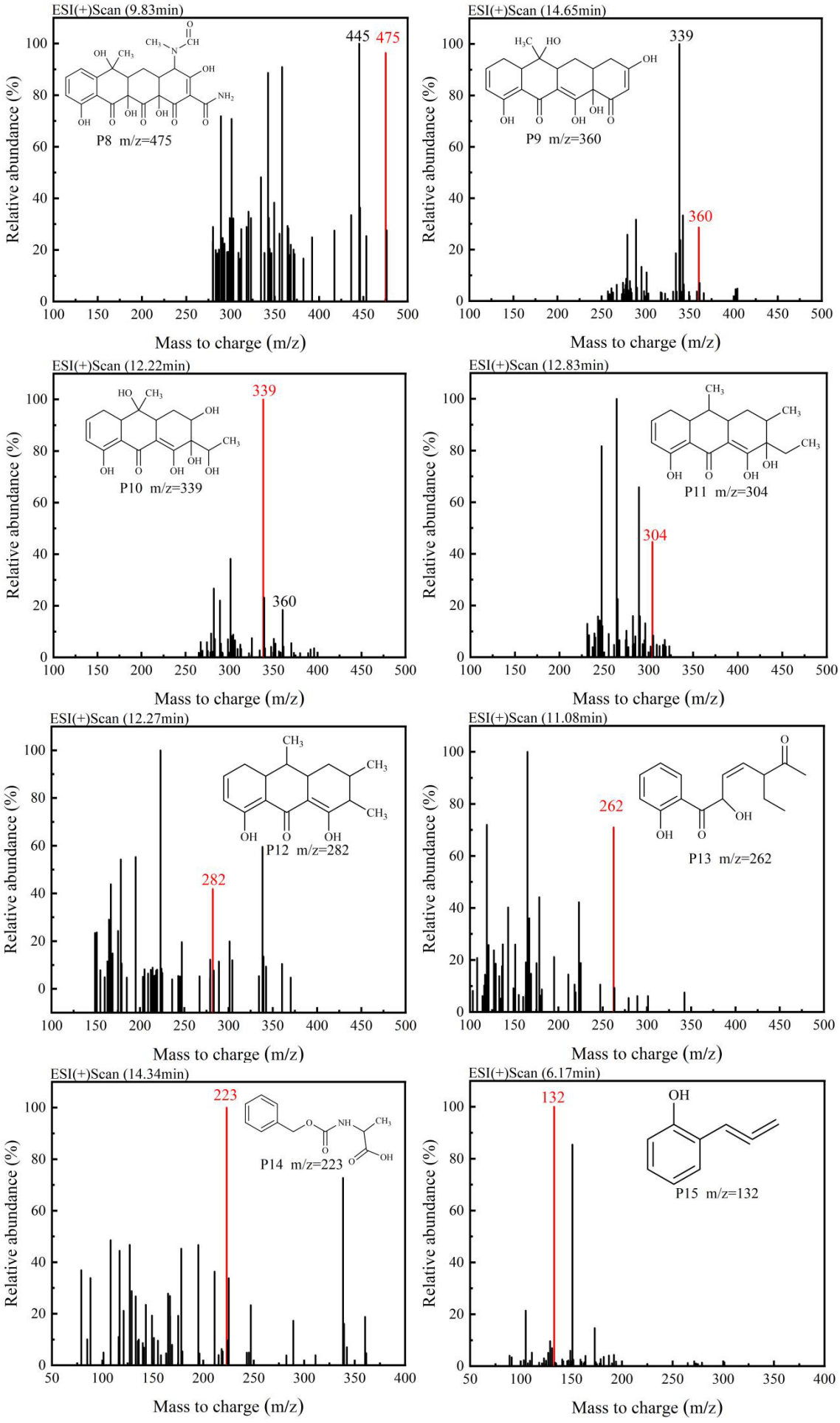
ESI(+)Scan (9.83min)
445
475
P8 m/z=475
ESI(+)Scan (14.65min)
339
360
P9 m/z=360
ESI(+)Scan (12.22min)
339
360
P10 m/z=339
ESI(+)Scan (12.83min)
304
P11 m/z=304
ESI(+)Scan (12.27min)
282
P12 m/z=282
ESI(+)Scan (11.08min)
262
P13 m/z=262
ESI(+)Scan (14.34min)
223
P14 m/z=223
ESI(+)Scan (6.17min)
132
P15 m/z=132
Relative abundance (%)
Mass to charge (m/z)

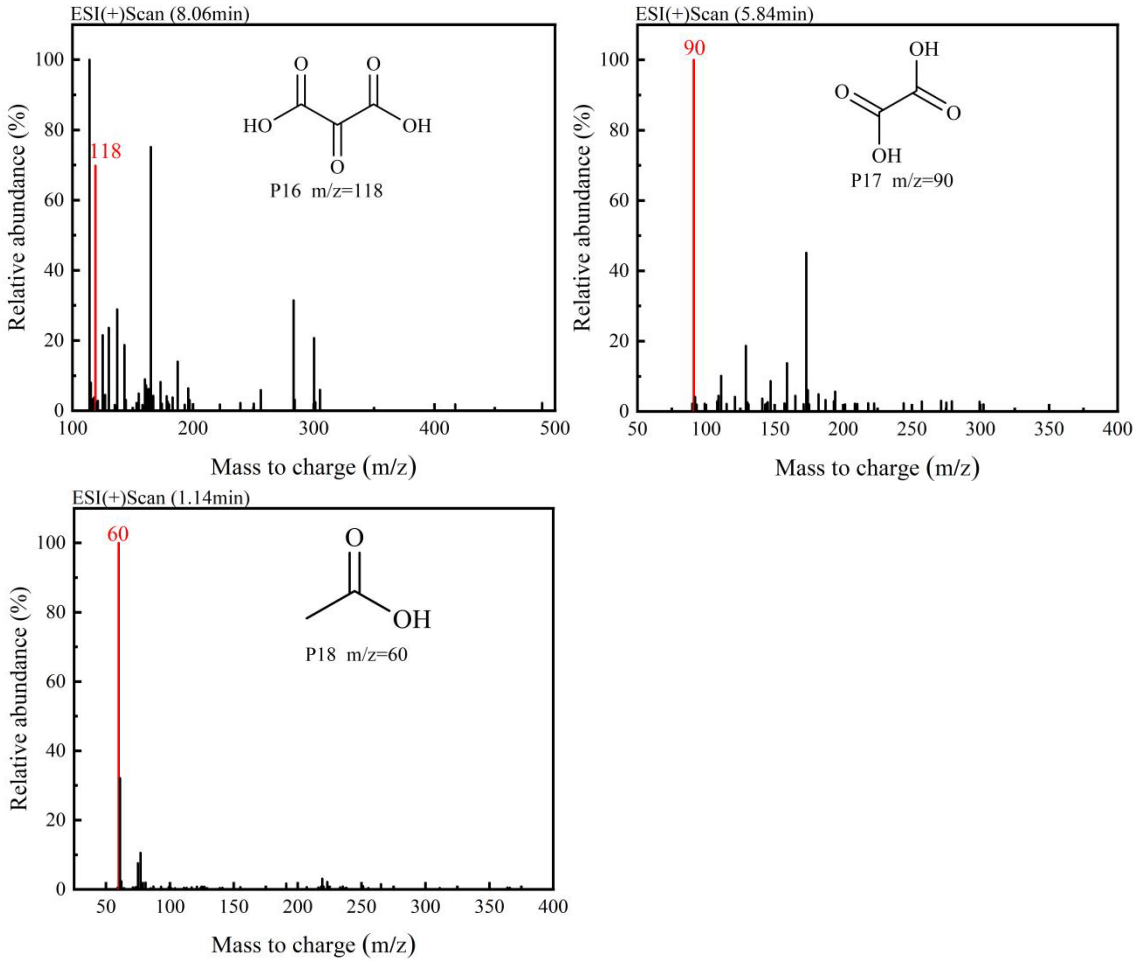

Figure S3. Mass spectrum of TC and its degradation intermediates.

Table S3. Mass spectrometry data for the identification of TC and its intermediates.

Compound list	Retention time (min)	Main fragment (m/z)	Chemical structure
TC	8.36	445	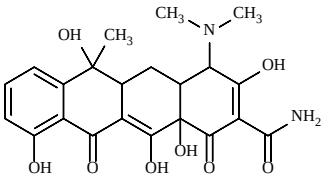
P1	7.28	461	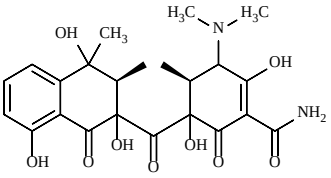
P2	9.37	477	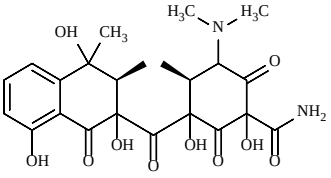
P3	10.24	459	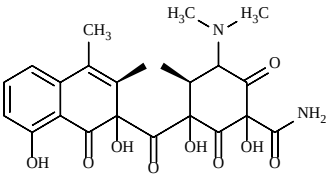
P4	9.17	417	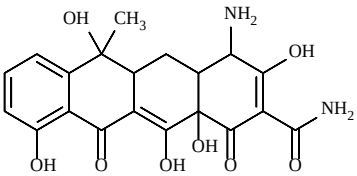
P5	13.36	339	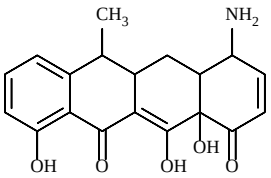
P6	4.86	325	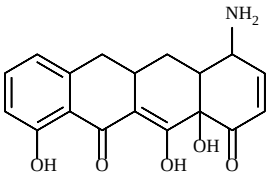
P7	7.33	171	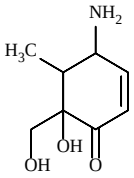

P8	9.83	475	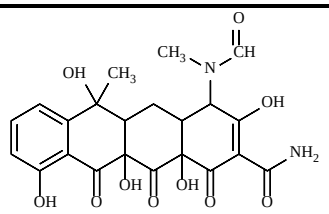
P9	14.65	360	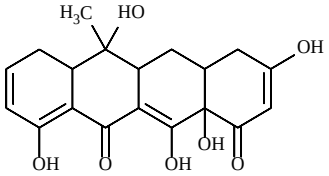
P10	12.22	339	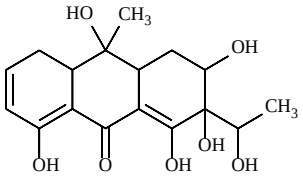
P11	12.83	304	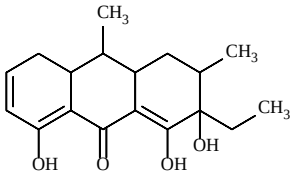
P12	12.27	282	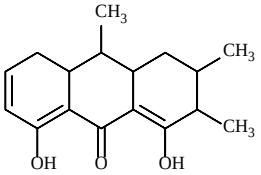
P13	11.08	262	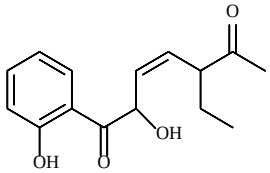
P14	14.34	223	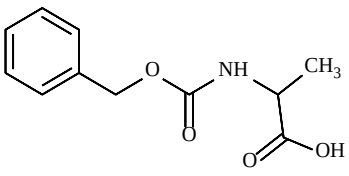
P15	6.17	132	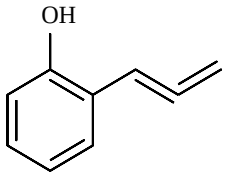
P16	8.06	118	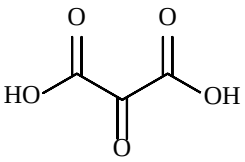

P17	5.84	90	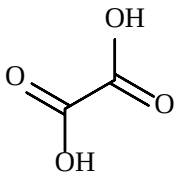
P18	1.14	60	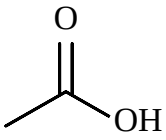

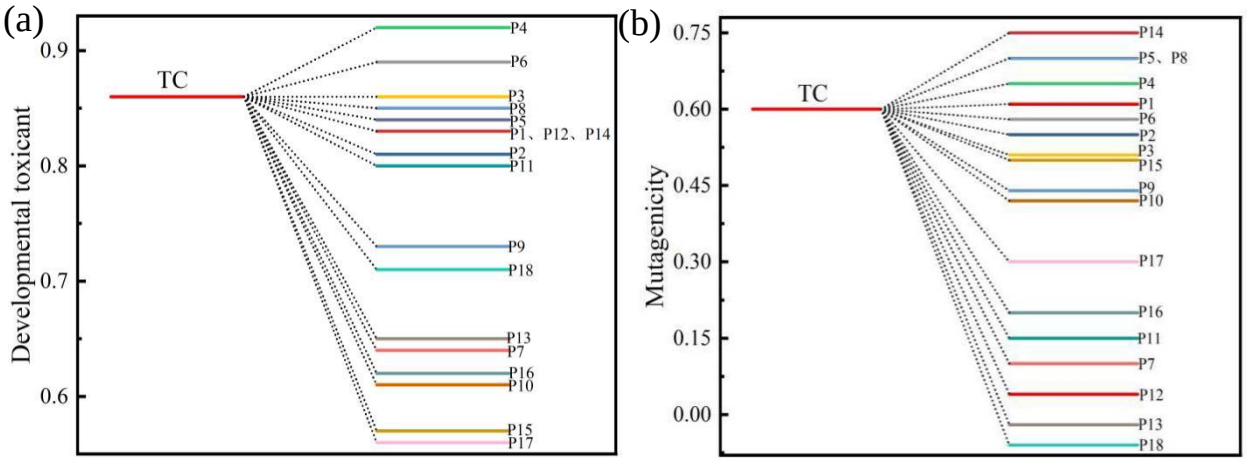

Figure S4. (a) The developmental toxicity and (b) mutagenicity of TC and its degradation intermediates predicted by the T.E.S.T. program.

Reference

[S1] X. Li, Y. Jia, J. Zhang, Y. Qin, Y. Wu, M. Zhou, J. Sun, Efficient removal of tetracycline by H2O2 activated with iron-doped biochar: Performance, mechanism, and degradation pathways, Chin. Chem. Lett. 33 (2022) 2105–2110. https://doi.org/10.1016/j.cclet.2021.08.054.

[S2] Y. Cao, K. Cui, Y. Chen, M. Cui, G. Li, D. Li, X. Yang, Efficient degradation of tetracycline by H2O2 catalyzed by FeOCl: A wide range of pH values from 3 to 7, Solid State Sci. 113 (2021) 106548. https://doi.org/10.1016/j.solidstatesciences.2021.106548.

[S3] Ultrathin iron-cobalt oxide nanosheets with enhanced H2O2 activation performance for efficient degradation of tetracycline, Appl. Surf. Sci. 535 (2021) 147655. https://doi.org/10.1016/j.apsusc.2020.147655.

[S4] L. Ge, Y. Yue, W. Wang, F. Tan, S. Zhang, X. Wang, X. Qiao, P.K. Wong, Efficient degradation of tetracycline in wide pH range using MgNCN/MgO nanocomposites as novel H2O2 activator, Water Res. 198 (2021) 117149. https://doi.org/10.1016/j.watres.2021.117149.

[S5] Q. Wu, H. Yang, L. Kang, Z. Gao, F. Ren, Fe-based metal-organic frameworks as Fenton-like catalysts for highly efficient degradation of tetracycline hydrochloride over a wide pH range: Acceleration of Fe (II)/ Fe (III) cycle under visible light irradiation, Appl. Catal. B Environ. 263 (2020) 118282. https://doi.org/10.1016/j.apcatb.2019.118282.

[S6] W. Zhong, Q. Peng, K. Liu, X. Tang, Y. Zhang, J. Xing, Building Cu0/CuFe2O4 framework to efficiently degrade tetracycline and improve utilization of H2O2 in Fenton-like system, Chem. Eng. J. 474 (2023) 145522. https://doi.org/10.1016/j.cej.2023.145522.

[S7] S. Huang, Q. Zhang, P. Liu, S. Ma, B. Xie, K. Yang, Y. Zhao, Novel up-conversion carbon quantum dots/α-FeOOH nanohybrids eliminate tetracycline and its related drug resistance in visible-light responsive Fenton system, Appl. Catal. B Environ. 263 (2020) 118336. https://doi.org/10.1016/j.apcatb.2019.118336.

[S8] Y. Xiong, X. Tang, Y. Liu, W. Li, Y. He, Y. Deng, Z. Lin, Y. Zhou, Activation of periodate by chalcopyrite for efficient degradation of tetracycline hydrochloride, Sep. Purif. Technol. 333 (2024) 125813. https://doi.org/10.1016/j.seppur.2023.125813.